Study of plasmid-based expression level heterogeneity under plasmid-curing like conditions in Cupriavidus necator

Catherine Boy, Julie Lesage, Sandrine Alfenore, Stéphane Guillouet, Nathalie Gorret

Version of Record: https://www.sciencedirect.com/science/article/pii/S0168165622000037
Manuscript_3db8a1890b909e260ad64042b7048e24

TITLE

Study of plasmid-based expression level heterogeneity under plasmid-curing like conditions in *Cupriavidus necator*

AUTHORS

Catherine BOY[1], Julie LESAGE[1], Sandrine ALFENORE[1], Stéphane E. GUILLOUET[1], Nathalie GORRET[1*],

[1] TBI, Université de Toulouse, CNRS, INRA, INSA, Toulouse, France

*CORRESPONDING AUTHOR

Nathalie GORRET

ngorret@insa-toulouse.fr

TBI, Université de Toulouse, CNRS, INRA, INSA, Toulouse, France

135 Avenue de Rangueil – 31077 Toulouse Cedex 04

ABSTRACT

Plasmid expression level heterogeneity in *Cupriavidus necator* was studied in response to stringent culture conditions, supposed to enhance plasmid instability, through plasmid curing strategies. Two plasmid curing strategies were compared based on their efficiency at generating heterogeneity in batch: rifampicin addition and temperature increase. A temperature increase from 30 to 37°C was the most efficient plasmid curing strategy. To generate a heterogeneous population in terms of plasmid expression levels, successive batches at supra-optimal culture temperature (*i.e.* 37°C) were initially conducted. Three distinct fluorescent subpopulations P_0 (not fluorescent), P_1 (low fluorescence intensity, median = 1 10^3) and P_2 (high fluorescence intensity, median = 6 10^3) were obtained. From there, the chemostat culture was implemented to study the long-term stress response under well-controlled environment at defined dilution rates. For dilution rates comprised between 0.05 and 0.10 h^{-1}, the subpopulation P_2 (62 % *vs* 90 %) was favored compared to P_1 cells (54 % *vs* 1 %), especially when growth rate increased. Our biosensor was efficient at discriminating subpopulation presenting different expression levels under stringent culture conditions. Plus, we showed that controlling growth kinetics had a stabilizing impact on plasmid expression levels, even under heterogeneous expression conditions.

KEYWORDS:

Plasmid curing, chemostat, plasmid stability, expression level, flow cytometry, Single-cell analysis

INTRODUCTION

Historically, microbial populations cultivated in assumed homogeneous environments are by extension also considered homogeneous in terms of its individuals. Nowadays, this postulate is being discussed and more and more studies showing that population heterogeneity can be observed among monoclonal cultures in homogeneous environments are being published (Carlquist et al., 2012; Delvigne and Goffin, 2014; Gonzalez-Cabaleiro et al., 2017; Heins and Weuster-Botz, 2018). In recombinant bioprocesses, population heterogeneity contributes to enhance process instability (Binder et al., 2017). Therefore, a better understanding of the mechanisms leading to phenotypic homogeneity of engineered strains is mandatory to ensure bioprocess robustness. In previous work (Boy et *al.*, 2020), a plasmid expression level monitoring method based on the expression of a plasmid-encoded eGFP biosensor has been designed, in order to identify subpopulations presenting different phenotypic behaviors. Its single-cell response to artificially induce plasmid expression level heterogeneity was studied in flasks through cell sorting through FACS (*i.e.* Fluorescence Activated Cell Sorting) technology. FACS allows the physiological characteristics of each subpopulation to be studied separately (*i.e.* growth rate) (Boy et al., 2020). As these experiments were performed in flasks with less than 20 cell generations, it would be interesting to increase the cell generation number submitted to plasmid curing-like conditions to amplify the heterogeneity in plasmid expression levels. In this work, the response of our plasmid expression level monitoring method in plasmid curing-like conditions is studied.

Plasmid curing strategies are developed to favor the removal of plasmids from bacterial cells, generally to obtain plasmid-free cells to study specific plasmid-encoded metabolisms (Andersen et al., 1981; Hughes et al., 1984; Monchy et al., 2006); or as a strategy to combat plasmid encoded antimicrobial resistance (Buckner et al., 2018; Zaman, 2010). The choice of the most appropriate curing agent for a plasmid vector is difficult to predict. Plasmids differ significantly in their ability to be cured based on their own properties. Thus, no universally effective curative agent has yet been identified. . (Trevors, 1986; Zaman, 2010). Many strategies have been developed over the years and are generally based on temperature increase (Andersen et al., 1981; Buckner et al., 2018; Hughes et al., 1984), plasmid incompatibility (Buckner et al., 2018; Trevors, 1986), antibiotic addition (*such as*. mitomycin C (Andersen et al., 1981; Hughes et al., 1984; Trevors, 1986), novobiocin (Trevors, 1986), rifampicin (Andersen et al., 1981; di Mauro et al., 1969; Hughes et al., 1984; Trevors, 1986)), addition of DNA

intercalating agents (*such as.* acridine orange (Andersen et al., 1981; Zaman, 2010)), acriflavine (Trevors, 1986), ethidium bromide (Andersen et al., 1981; Zaman, 2010)), or detergent additions (*such as.* sodium dodecyl sulphate (Andersen et al., 1981; Zaman, 2010)). In most protocols, plasmid curing techniques are coupled with successive subcultures under these stringent conditions. *Cupriavidus sp.* homologous plasmids have already been removed by some of these methods: acridine orange, ethidium bromide, sodium dodecyl sulfate (Andersen et al., 1981), benzoate (Hughes et al., 1984), rifampicin, mitomycin C and higher growth temperature (Andersen et al., 1981; Hughes et al., 1984). In this work, attention was drawn to rifampicin addition and temperature increase.

Rifampicin addition as plasmid curing strategy was interesting in our case of study, as it causes variations in the plasmid expression level through disruption in DNA transcription. Rifampicin was shown to bind and consequently to inhibit RNA polymerase molecule, the enzyme responsible for DNA transcription by forming a stable drug-enzyme complex (Wehrli, 1983). In Bazzicalupo et *al.* (1972), rifampicin specifically inhibited the initiation step in the reaction catalyzed by RNA polymerase, therefore eliminating the F'-lac plasmid from *E. coli*. Studies showed that plasmids seemed to have been completely cured from *Escherichia coli* (Haemolysin and F'-lac plasmids (Buckner et al., 2018)), *Staphylococcus aureus* (Penicillinase plasmids (Buckner et al., 2018; Trevors, 1986)) and *Cupriavidus necator* (100 $mg \cdot L^{-1}$ for Hydrogenase plasmids (Andersen et al., 1981)). Nevertheless, rifampicin did not allow curing plasmid from *E. coli* strains whose RNA polymerases were rifampicin-resistant (Bazzicalupo and Tocchini-Valentini, 1972; Buckner et al., 2018; di Mauro et al., 1969; Trevors, 1986).

Increasing growth temperature from 5 to 7°C above the optimal growth temperature was used as an effective curing strategy. The mechanisms of thermal curing of plasmids are not well known. Hypotheses suggest that the application of temperatures above the optimum operating temperature of RNA polymerases could directly interfere with plasmid replication mechanisms. This curing strategy was coupled with series of subcultures using successive inoculations when log phase has been reached (Trevors, 1986). Several cell generations have to be generated in order to be efficient. In *C. necator*, a growth temperature of 42°C (12 degree above optimal growth temperature) was successfully applied for curing plasmids (Hughes et al., 1984).

Cupriavidus necator has regained much interest in recent years, due to its natural metabolic potentialities such as both autotrophic and heterotrophic growth (Budde et al., 2011; Crepin et al., 2016; Friedrich et al., 1979; Grousseau et al., 2014; Grunwald et al., 2015; Johnson, 1971; Marc et al., 2017), and as its poly-β-hydroxybutyrate (PHB) biosynthesis pathways (Cruz et al., 2019; Koller et al., 2010; Nangle et al., 2020;

Pohlmann et al., 2006; Tang et al., 2020). Especially, synthetic biology and metabolic engineering have been implemented in order to build heterologous metabolic pathways for synthon biosynthesis (Black et al., 2018; Crepin et al., 2016; Ewering et al., 2006; Garrigues et al., 2020; Grousseau et al., 2014; Hoefel et al., 2010; Krieg et al., 2018; Marc et al., 2017; Muller et al., 2013). In that context, it is crucial to develop and validate tools to be able to evaluate the robustness of strain within a bioprocess.

In order to further evaluate our capacity to monitor the heterogeneity of plasmid expression level at the single-cell level, *C. necator* strains bearing an engineered eGFP-biosensor plasmid were submitted to two plasmid curing conditions (temperature increase and rifampicin addition) to artificially induce heterogeneity. Herein we aimed at studying more precisely the response of the biosensor under various cultivation modes (batch and chemostat) and investigating the impact of growth rate on plasmid expression level heterogeneity. First, the two plasmid curing strategies were led in batch mode to evaluate their impact on cell physiology (subpopulations) and cell macroscopic behavior. Then, the most efficient plasmid curing strategy was applied in chemostat.

MATERIAL AND METHODS

Strain, plasmids and media

Strains

C. necator Re2133 (Budde et al., 2011) was chosen as expression strain. It was derived from the wildtype strain *C. necator* H16 / ATCC17699 whose genes encoding for acetoacetyl-CoA reductases (*phaB1B2B3*) and for PHA synthase (*phaC1*) were deleted. *Cupriavidus necator* is naturally resistant to gentamicin. Plasmid constructions were achieved through the strains *Escherichia coli* S17-1 (ATCC 47055) and Top10 (InvitrogenTM, Life technologies).

Plasmids

The plasmid CB1 was used in this work. This plasmid encodes for an eGFP through the insertion of the P_{lac}-*egfp* cassette (Gruber et al., 2014) on the pBBad (Fukui et al., 2009) backbone, derived from the pBBR1MCS-2 plasmid (Kovach et al., 1995), which bears kanamycin resistance (Kan^R). Its design and associated molecular biology protocols were described in more details in Boy et *al*. (2020).

Media

The rich medium used for precultures was Tryptic Soy Broth (TSB, 27.5 $g \cdot L^{-1}$, Becton Dickinson, Sparks, MD, USA). Gentamicin (10 $mg \cdot L^{-1}$) and kanamycin (200 $mg \cdot L^{-1}$) were added as final concentrations to ensure purity of the culture and plasmid stability, respectively. To prepare Tryptic Soy Agar (*abbr.* TSA) plates, TSB medium was supplemented with 20 $g \cdot L^{-1}$ agar.

For molecular biology, the rich Lysogeny broth medium (*abbr.* LB) was used (10 $g \cdot L^{-1}$ peptone, 5 $g \cdot L^{-1}$ yeast extract, 10 $g \cdot L^{-1}$ NaCl). Same as above, LB medium was supplemented with 20 $g \cdot L^{-1}$ agar to produce LB agar plates.

The mineral medium for flasks cultivation was detailed in Lu et *al.* (Lu et al., 2013). Gentamicin (10 $mg \cdot L^{-1}$) and kanamycin (200 $mg \cdot L^{-1}$) were added to this medium. The carbon and nitrogen sources used were respectively fructose (20 $g \cdot L^{-1}$) and NH_4Cl (0.5 $g \cdot L^{-1}$).

The mineral medium used for bioreactor cultivation was composed as follows (per liter): $(NH_4)_2SO_4$, 2.8 g; $MgSO_4$-$7H_2O$, 0.75 g; rich phosphorus solution (Na_2HPO_4-$12H_2O$, 1.50 g; KH_2PO_4, 0.25 g); nitrilotriacetic acid, 0.285 g; ammonium iron(III) citrate (28%), 0.090 g; $CaCl_2$, 0.015 g; trace elements (H_3BO_3, 0.45 mg; $CoCl_2$-$6H_2O$, 0.30 mg; $ZnSO_4$,$7H_2O$, 0.15 mg; $MnCl_2$-$4H_2O$, 0.045 mg; Na_2MoO4-$2H_2O$, 0.045 mg; $NiCl_2$-$6H_2O$, 0.03 mg; $CuSO_4$, 0.015 mg). Fructose (30 $g \cdot L^{-1}$) was used as carbon source.

Inoculum Preparation

Inoculum preparation was performed exactly as described in Boy et *al.* (2020).

Plasmid curing during batch cultivations on fructose

Batch cultivations in multi-instrumented 5 L bioreactor Biostat®B-DCU (Sartorius, Germany) were carried out as described in Boy et *al.* (2020). Temperature (30 - 42°C), pH (7) and partial pressure of dioxygen (pO2 > 30 %) in the medium could be controlled throughout culture.

Initial fructose concentration in medium was 50 $g \cdot L^{-1}$ and pulses of both rich phosphorus solution (7 $mL \cdot L^{-1}$) and trace elements solution (2 $mL \cdot L^{-1}$) were performed every 10 $g \cdot L^{-1}$ of biomass produced to prevent nutrient depletion.

After reaching a concentration of 7.5 $g_{CDW} \cdot L^{-1}$ of biomass in the bioreactor, plasmid curing strategies were applied: either by an addition of 50 $mg \cdot L^{-1}$ of rifampicin or an increase of the temperature of culture up to 42°C.

Successive batch subcultures from 30 to 37°C

To generate population heterogeneity prior the start of the continuous culture, successive batch subcultures were made. Batch cultivations were performed as detailed above with an initial fructose concentration of 10 $g \cdot L^{-1}$. The first batch was carried out at 30°C until fructose was completely consumed, 900 mL fermentation broth was then withdrawn through a peristaltic pump and 900 mL of fresh bioreactor mineral medium were added in the bioreactor. Temperature was increased at 37°C. For the seven next batches at 37°C, the protocol was the same. After the eighth batch at 37°C, the chemostat cultivation was started.

Plasmid curing during continuous cultivation on fructose

Fructose-limited continuous culture was established by feeding the bioreactor with fresh medium (Bioreactor mineral medium supplemented with 10 $g \cdot L^{-1}$ fructose). In chemostat-modes, 2 dilution rates were investigated at 0.05 and 0.10 h^{-1} respectively.

Steady state conditions were reached after at least five residence times (*i.e.* 0.05 h^{-1}, 100 h and 7.21 cell generations; 0.10 h^{-1}, 50 h and 7.21 cell generations). The steady state phase was assessed through constant measurements of biomass and residual fructose concentrations, as well as stable composition of the exhaust gases. Temperature was set at 37°C, and pH was regulated at 7. The partial pressure of dioxygen was maintained at 30 % of the saturation through aeration and stirring regulation.

Analytical procedure

Biomass characterization

Biomass concentration was measured by optical density (OD) at 600 nm using a visible spectrophotometer (DR3900, Hachlange, Loveland, Colorado, USA) with a 0.2 cm path length absorption cell (Hellma). OD was correlated to cell dry weight (CDW) measurements (*i.e.* 2 $g_{CDW} \cdot L^{-1}$ = 1 OD unit). For cell dry weight measurements, 0.2 µm pore-size polyamide membranes (Sartorius, Göttingen, Germany), were beforehand dried (60°C, 200mmHg, 72 h) and weighted. Culture medium was sampled and filtrated on dried membranes which were dried again in the same conditions.

Metabolite quantification

Cells samples were centrifuged, and supernatants were filtrated (0.2 µm PTFE syringe filters, VWR) before being used for substrate and products determination. The residual fructose concentration was quantified by high-performance liquid chromatography (HPLC). Other metabolites were searched using the same protocol and calibration curve were set for acetic, formic, propionic, pyruvic succinic acids. The HPLC instrument (Series 1100, Agilent) was equipped with an ion-exchange column (Aminex HPX-87H, 300×7.8 mm, Bio-Rad, Hercules, CA, USA) protected with a guard column (Cation H+ cartridge, 30×4.6 mm, Bio-Rad) and coupled to a RI detector and an UV detector (λ=210 nm). The column was eluted with 2.5 mM H_2SO_4 as a mobile phase at 50 °C at a flow rate of 0.5 mL·min^{-1}. Residual nitrogen was quantified by higher-pressure ionic chromatography (HPIC). The HPIC instrument (ICS-2100 RFIC, Dionex) was equipped with an IonPac™ CS16 column (RFIC™, 3x50mm, BioRad) and an ion suppressor CERS 500 (2 mm, Thermo Scientific). The column was eluted with 30 mM methanesulfonic acid as a mobile phase at 40 °C and a 40 mA ion suppressor current, at a flow rate of 0.36 mL·min^{-1}.

Plate count

C. necator is naturally resistant to gentamycin and plasmid-bearing cells are resistant to kanamycin. Plasmid stability was quantified by parallel plate count on antibiotic selective TSB Petri dishes (10 mg·L^{-1} Gentamicin and 10 mg·L^{-1} Gentamicin + 200 mg·L^{-1} Kanamycin). Serial dilutions were performed in physiological water (0.85 % NaCl) tubes (BioMérieux, Marcy-l'Étoile, France). For every sample, three dilutions were tested, between 10^{-5} and 10^{-9}. The diluted samples were plated in triplicate with the Whitley Automated Spiral Plater (Don Whitley Scientific, Shipley, UK). The results of cell plate counting method were reproducible within 10% based on 3 dilutions in triplicate.

From these data, the decimal reduction rate of plasmid-expressing cells was calculated as the ratio of the concentration of total cells (Gen^R) on the concentration of plasmid-expressing cells (Gen^RKan^R); this ratio was converted to logarithm.

Flow cytometry

Cell permeability (FL3 fluorescence channel) and eGFP-fluorescence (FL1 fluorescence channel) were measured at single-cell level with the BD Accuri C6® flow cytometer (BD Biosciences, Franklin Lakes, NJ, USA). Samples were diluted in physiological water to 10^6 cells mL^{-1}. Samples were run until 20, 000 events were counted at 14 µL·min^{-1} using milli-Q water as sheath fluid. The Forward Scatter Signal (threshold: 12,

000) and Side Scatter Signal (threshold: 2, 000) were used as trigger channels. Data acquisition was performed with BD Accuri CFlow® software. Data processing was achieved with FlowJo software (Becton Dickinson, Sparks, MD, USA). Events consider as *C. necator* cells (total cells) were gated based on a double-singlet gating method, selecting only cells situated on the bisectors of both the (FSC-A vs. FSC-H) and (SSC-A vs. SSC-H).

For the quantification of permeable cells, propidium iodide (PI) (Molecular probes, Invitrogen, USA) was used. After dilution, cell samples were stained with 20 µL of the commercial solution at 1 $mg \cdot L^{-1}$ PI and incubated 20 minutes at room temperature in the dark. A 100 % dead–cell control (100% permeable cells) was prepared by incubating cells in 70 % isopropanol for 1 h at room temperature. The % of permeabilized cells was determined as being the ratio between the number of PI labelled cells and of total cells.

For the analysis of the distribution of eGFP-fluorescence cells, fluorescence intensity was measured at single-cell level on the FL1 fluorescent channel. Decimal reduction rate was calculated as described above from plasmid-expressing cells (eGFP-positive cells; FL1-A > $8 \cdot 10^2$) and total cells. The eGFP-subpopulations P0, P1, P2 were defined based on (FL1-A) fluorescence intensity distribution within the total cells as the one described in Boy et al., 2020.

Extracellular fluorescence measurement

Samples were centrifuged 3 min at 13, 000 rpm with a MiniSpin® table-top microcentrifuge (Eppendorf, Germany) to remove cells from the liquid. The extracellular fluorescence intensity in the supernatant was measured with the Synergy™ HT (Biotek®, USA) multiplate reader at excitation wavelength 485 ± 20 nm and emission wavelength 525 ± 20 nm at sensitivity of 50. Black Nunclon® 96-well plates (ThermoFisher, USA) were used.

Statistical analysis: Normality of distribution functions by BoxPlot representation

The boxplot method aims at representing data distribution through the graphical depiction of its main statistical features, such as the median (50^{th} percentile), the first (25^{th} percentile) and third quartiles (75^{th} percentile). The first and third quartiles correspond to the bottom and top of the boxplot, respectively. The line inside the boxplot symbolizes the median. The interquartile range (*abbr.* IQR) between the first and third quartiles represents the length of the boxplot. The whiskers symbolize the minimum and maximum values as long as they are located within 1.5 x IQR from both extremities of the box. Above 1.5 x IQR, outliers are represented by points (Boy et

al., 2020). A symmetric boxplot centered on the median is commonly considered as normally distributed (Rakotomalala, 2011).

Data analysis

The error on the specific growth rate (determined as being the slope of $\ln[g_{CDW} \cdot L^{-1}] = f(t)$ for batch on dry mass) was calculated as the standard deviation (SD) of the slope. For the yield determination, the state variables (concentrations for batch or weights for fed-batch) were plotted pairwise in a scatter plot within the considered period of the culture. A linear regression was applied to determine the yield (as the slope) and the error (as the SD of the slope).

RESULTS

In order to evaluate our capacity to monitor heterogeneity in plasmid expression level at the single-cell level, the *C. necator* strain Re2133 was transformed with the biosensor-encoding plasmid (pCB1) (Boy et al., 2020). Cell population was analyzed by flow cytometry throughout the cultivation in order to get access to single-cells analysis. Therefore, the distribution of plasmid expression levels could be analyzed in relation to fluorescence intensity distribution within the entire population. As it was previously demonstrated that the plasmid pCB1 presented a low metabolic burden on *C. necator* Re2133 host cells (Boy et al., 2020), any variations detected in the plasmid expression could be attributed to external factors, like plasmid curing strategy, or variations in dilution rate.

Plasmid curing strategy suitable with expression level monitoring during batch cultures

Two different plasmid curing strategies, temperature increase and rifampicin addition, were carried out in batch mode with the strain Re2133/pCB1 in order to define the most efficient method to enhance heterogeneity in plasmid expression. Analyses were supported by macroscopic data (*e.g.* growth kinetics, yields) and population heterogeneity description.

Impact of rifampicin addition and temperature increase on the growth of C. necator Re2133/pCB1 in batch

For the rifampicin-based strategy, preliminary cultures in flasks were achieved beforehand in order to evaluate the concentration of rifampicin needed in the bioreactor to induce plasmid curing (*data not shown*), concentrations from 50 to 150 $mg \cdot L^{-1}$ were tested. A concentration of 50 $mg \cdot L^{-1}$ rifampicin allowed the highest

reduction in the number of plasmid-expressing cells without completely inhibiting growth. For the temperature-based strategy, temperature regulation was set at 42°C, based on previous experiments described in the literature (Andersen et al., 1981; Trevors, 1986).

For both strategies, cultivations in bioreactors were achieved under optimal culture conditions up to 7.5 $g_{CDW} \cdot L^{-1}$ of biomass in the bioreactor. Then, plasmid curing was induced in both bioreactors.

The specific growth rates during the different phases were determined from the biomass concentration evolution (**Table 1**). After rifampicin addition, the specific growth rate dropped to 0.09 ± 0.01 h^{-1}. After temperature increase, growth rate was drastically reduced to 0.009 ± 0.001 h^{-1}. Once biomass reached a concentration of 10 $g_{CDW} \cdot L^{-1}$ (6.6 cell generations), temperature was set back at 30°C to verify the reversibility of the phenomenon. Growth rate remained greatly diminished and only reached 0.04 ± 0.01 h^{-1} after 13 h (about 1 generation).

Biomass production yields (**Table 1**) were evaluated from fructose consumption concentrations and compared to theoretical data 0.53 $g.g^{-1}$ (Aragao, 1996). As expected, before plasmid curing induction, the overall biomass production yields were comparable for both cultures, within 0.47 ± 0.02 $g_X \cdot g_S^{-1}$, and rather close to the theoretical yield. However, after plasmid curing induction, yield values decreased for both strategies. The reduction rate was more important after temperature increase (-62%) than after rifampicin addition (-27%). After switching temperature back to 30°C, yield seemed to be recovered close to the theoretical reference value, even when the growth rate was still affected.

Subpopulation characterization

Plasmid expression level monitoring

The fluorescence intensity distribution of eGFP fluorescent cells was measured by flow cytometry in order to quantify different expression levels. Boxplots have been chosen to represent fluorescence intensity distributions. Distributions of population are represented versus both the generation number and the time course of the culture. Data were presented according to cell generations, in order to compare experiments regardless of growth dynamics and to highlight the number of time cells were divided instead of the duration of the experimentations.

Under optimal culture conditions, fluorescence intensity distribution was Gaussian for both cultures, as the first and third quartiles had equal lengths, and as the mean and median values were equal (**Figure 1**). Plasmid curing conditions were induced after 5.9 generations. For plasmid curing by rifampicin addition (**Figures 1a** & **b**), the

first quartile widened showing a slight sliding of the fluorescence intensity distribution toward lesser fluorescent cells. For plasmid curing by temperature increase at 42°C (**Figures 1c** & **d**), fluorescence intensity distribution widened globally and the median slipped toward lower fluorescence intensity distribution. This phenomenon seemed to be partly reversible as median increased again when temperature was set back to 30°C. This was not due to a change in the quantum yield of eGFP at 42°C and 30°C, as it was verified that eGFP was not impacted by temperature increase at 42°C. To do this, supernatant samples were incubated at 42°C for 24 h, and no variation in the value of fluorescence intensity was detected compared to 37°C (*data not shown*). For an equal generation number between both plasmid curing conditions, the associated culture length is way longer for temperature increase (70 h), as growth rate was highly diminished, compared to rifampicin addition (25 h).

Plasmid stability

Plasmid expression stability was evaluated through flow cytometry and plate count. A gap in cell concentrations between plate count and flow cytometry might reveal a cultivability loss, due to the side effects of plasmid curing on the physiology of host cells. In addition, the dynamic of plasmid expression was evaluated through decimal reduction rates.

In the rifampicin experiment (**Figure 2a**), concentrations of total cells and of cells expressing the plasmid were consistent both by plate count and flow cytometry throughout the culture; meaning gentamicin resistant cell concentration (Gen^R) was equal to single-cell concentration, and that gentamicin and kanamycin resistant cell concentration (Gen^RKan^R) was equal to eGFP-positive cell concentration. The cultivability was not reduced by rifampicin addition. The specific growth rate calculated from the single-cells concentration by flow cytometry was compared to the one determined from the cell dry weight, described beforehand. Growth rate by flow cytometry was evaluated at 0.24 ± 0.03 h^{-1} under optimal growth conditions, and at 0.06 ± 0.05 h^{-1} after plasmid curing induction. Even if growth rate evaluation was noisier by flow cytometry, the orders of magnitude reached was once again equivalent. Thus, flow cytometry and cell dry weight measurements gave comparable growth dynamics. The decimal reduction rate (**Figure 2c**) remained lower than 0.05 for both counting methods confirming that there was no significant decrease in the plasmid expression due to rifampicin addition.

In the temperature experiment (**Figure 2b**), total and plasmid-expressing cell concentrations were consistent both by plate count and flow cytometry under optimal growth conditions. After plasmid curing induction, the gap between the two counting methods increased reaching a one-decade difference for both plasmid-expressing cell and total cell populations. Growth considerably slowed down and cell concentration even decreased for both

Gen^R and Gen^RKan^R populations, which might confirm that cell cultivability decreased at 42°C. When temperature was set back to 30°C after 6.6 cell generations, cell concentration increased slightly for both counting methods and both cell populations. Returning to optimal temperature conditions has prevented further decrease in cell cultivability, but did not allow a complete recovery of cells, as they were not able to grow at their original rate. Like for rifampicin, the growth rate from flow cytometry was compared to growth rate from cell dry weight. Growth rate by flow cytometry was evaluated at $0.23 \pm 0.04\ h^{-1}$ under optimal growth conditions, at $0.004 \pm 0.004\ h^{-1}$ after plasmid curing induction and at $0.03 \pm 0.05\ h^{-1}$ after temperature was set back to 30°C, consistent with the ones calculated from biomass.

Decimal reduction rate (**Figure 2d**) reached a maximum value of 0.18 for plasmid curing by temperature increase and 0.06 by rifampicin. Batch conditions were identical as both precultures were led exactly in the same manner; permeability as well as fluorescence levels were also verified to be identical before bioreactor inoculation. A low decimal reduction rate was measured before plasmid curing induction, either by temperature or rifampicin, by both counting methods: flow cytometry and plate count. After thermal plasmid curing induction, decimal reduction rate increased from 0 to 0.16 by flow cytometry, and from 0.04 to 0.15 by plate count. This value stabilized around 0.18 by both counting methods after temperature decrease. No significant increase was detected after rifampicin addition, by both counting methods.

Plasmid expression loss increased significantly after plasmid curing induction. When comparing plasmid curing strategies, it appears obvious that temperature increase presented the most negative effect on the cell concentration for plasmid-expressing and total cell populations, and consequently on the decimal reduction rate. This negative impact was more notable on plate count measurements, certainly due to cultivability loss.

Cell permeability and eGFP leakage

To further investigate cell physiology, cell permeability and eGFP leakage in the medium were investigated (**Figure 3**). Under optimal culture conditions, the percentage of permeabilized cells was low (% PI - positive cells < 5 %) for both experiments. The higher RFU value at the beginning of the batches might be due to a higher eGFP leakage in flasks precultures. Relative extracellular fluorescence intensity (*i.e.* extracellular fluorescence intensity normalized by optical density at 600 nm) decreased, because optical density increased significantly faster than extracellular fluorescence intensity. This was consistent with low cell permeabilization **(Figure 3)** and the stable normal fluorescence intensity distribution showed above (**Figure 1**). Therefore, eGFP

excretion in the medium was low under optimum culture conditions. Initial optical density and fluorescence intensity in the supernatant were taken as reference to calculate relative fluorescence intensity in the medium.

After rifampicin addition (**Figure 3a**), the percentage of permeabilized cells remained low. The relative extracellular fluorescence intensity was constant, meaning that the amount eGFP excreted by cells became constant and stable.

After temperature increase (**Figure 3b**), the percentage of permeabilized cells increased quickly up to 10 %. The relative extracellular fluorescence intensity increased abruptly. Since cell growth had stopped, the increase in relative extracellular fluorescence was only due to enhanced cell permeabilization. As a result, the fluorescence intensity distribution decreased in single-cells (**Figure 1**). Thus, single-cells excreted more eGFP as the percentage of permeabilized cells increased. When temperature was set back to 30°C, cell permeabilization percentage decreased, because the newly formed cell population was not permeable and so, overthrown the cell population permeabilized by temperature. Meanwhile, relative extracellular fluorescence intensity decreased. Temperature increase led to an enhanced eGFP leakage outside of cells, but this phenomenon could be slowed down by returning to optimal temperature.

The most appropriate approach to generate population heterogeneity had to be selected for further experiments. Plasmid curing by temperature led to a significant decrease in the plasmid expression levels (increase of decimal reduction rate), which was not the case with rifampicin addition. It might be partially due to too stringent culture conditions as shown by high cell permeabilization percentage and cultivability loss by plate count. Both strategies led to decreased growth rate. However, temperature increase at 42°C almost completely inhibited growth. Therefore, temperature increase was the most promising method to induce population heterogeneity. However, to avoid too high cell permeabilization and cultivability loss, the setpoint temperature for the following experiments had to be slightly decreased at 37°C.

Plasmid expression level monitoring during continuous culture at supra-optimal temperature

In order to study the impact of the dilution rate (*i.e.* growth rate) on the stability of the plasmid expression, eGFP fluorescence was measured in cells cultivated in chemostat under fructose limitation and under plasmid-curing conditions (i.e. temperature increase). It has been reported that the plasmid replication rate and / or plasmid copy number could be regulated by the dilution rate in chemostat (Klumpp, 2011; Koizumi et al., 1985; Reinikainen and Virkajärvi, 1989).

The combination of plasmid curing and chemostat mode should make it possible to create more cell generations (hopefully to amplify the phenomenon observed in batch mode) and to study the impact of the dilution rate (*i.e.* growth rate) on plasmid stability.

As mentioned above, the chemostat temperature was set at 37°C instead of 42°C, representing a 7°C - increase from the optimal temperature, which was advised for plasmid-curing experiments (Trevors, 1986). This temperature condition had already been applied in our previous work for plasmid curing during successive subcultures in flasks (Boy et al., 2020). In such condition, three different subpopulations were discriminated based on their fluorescence intensity distribution after 19 cell generations: P_0 (no fluorescence), P_1 (low fluorescence intensity, median value in FL1-H = $1 \cdot 10^3$) and P_2 (high fluorescence intensity, median value in FL1-H = $6 \cdot 10^3$). Subpopulations P_1 and P_2 presented a difference in their specific growth rates in 96 - well plates in double selective medium (*i.e.* gentamicin + kanamycin) with 0.09 ± 0.03 h^{-1} and 0.05 ± 0.01 h^{-1}, respectively (Boy et al., 2020).

Successive batches

First, a batch culture was led at 30°C in order to set the reference condition. This reference condition was characterized by 100 % eGFP - positive cells whose fluorescence intensity distribution was centered on the median of the subpopulation P_2 (= $6 \cdot 10^3$). Then, successive batch cultures were carried out in the same bioreactor at 37°C until the three subpopulations P_0, P_1 and P_2 as defined above appeared. Then, chemostat was started at a dilution rate of 0.05 h^{-1}.

Growth rate during successive batches varied significantly depending on the culture conditions applied (**Table 2**). At 30°C, growth rate was maintained at 0.25 ± 0.01 h^{-1}, which was consistent with optimal culture conditions for this strain. Then, during the first batch at 37°C, the specific growth rate dropped to 0.06 ± 0.01 h^{-1}. This was the lowest specific growth rate observed, since it increased in the next batches from 0.15 ± 0.01 to 0.22 ± 0.01 h^{-1}. So, in the last 37°C - batch, the specific growth rate was only 20 % lower to its value at 30°C.

At the end of the batch at 30°C, the whole cell population remained stable mainly in the subpopulation P_2 gate (**Figures 4a** & **5**), corresponding to the fluorescence intensity distribution under optimal culture conditions. The fluorescence intensity distribution remained symmetric and narrow around the median until the end of the 30°C batch (**Figure 5**).

At the beginning of the first 37°C batch, the median of the fluorescence intensity distribution quickly reached $4 \cdot 10^3$ again in the FL1-H channel. The distribution range was wider than during the 30°C batch. Between 0 and 15 cell generations, the fluorescence intensity distribution remained mostly in the P_2 subpopulation gate (**Figure 5**), but its distribution range increased throughout this time-period (**Figure 4a**). After 15 cell generations, the distribution range increased drastically towards the lower fluorescence intensity, which was confirmed by the increase in the percentage of P_1 fluorescent cells (**Figure 6**). After 30 cell generations, subpopulations P_1 and P_2 were clearly obtained, each one representing approximately 50 % of the eGFP-positive cell population. At that stage, it was decided to switch to chemostat mode.

Plate count was performed at the end of each batch (**Figure**7**b**). For flow cytometry measurements, only endpoints of each batch were shown (**Figure 7a**). The results for flow cytometry and plate count analysis gave cell concentrations comprised in the same order of magnitude. During successive batches, cell concentration reached around 10^{10} cells·mL^{-1} both by plate count and flow cytometry.

During the successive batches (until 30 generations), the decimal reduction rate (**Figure 7d**) obtained for $Gen^R Kan^R$ cells remained close to zero, meaning that all cells present in the bioreactor were bearing the plasmid, even without selection pressure in the bioreactor. Decimal reduction rate for P_2-cells also remained close to zero (**Figure 7c**), but this value started increasing after 15 cell generations up to 0.25. This corresponded to the decrease of the decimal reduction rate for P_1 and P_0 - cells. During the first 15 generations, the decimal reduction rate for P_1 and P_0-cells was higher, around 1.0-1.5 and 1.5-2.2 respectively.

Chemostat at 0.05 h^{-1}

First, a low dilution rate of 0.05 h^{-1} was set, which was close to the lowest specific growth rate obtained during successive batches at 37°C and close to the specific growth rate of P_2-cells (0.07 ± 0.02 h^{-1}) determined on selective medium (gentamicin + kanamycin) in 96 - well plates (Boy et al., 2020). The 0.05 h^{-1} - chemostat was carried out at 37°C for 340 h, corresponding to 27 cell generations. At the macroscopic level, the total biomass concentration expressed as dry cell weight and OD_{600nm} was maintained constant at 5 $g_{CDW} \cdot L^{-1}$ (*i.e.* 2.5 OD_{600nm}). In addition, no significant changes of metabolism were identified based on extracellular metabolites (*i.e.* no metabolites detected by HPLC) and exhausted gas analyses. Based on those macroscopic analyses, the steady state was reached after 35 generations (7.2 generations after the start of 0.05 h^{-1}-chemostat) and still settled after 20 more generations.

Nevertheless, based on single-cell level analysis, it was possible to show an evolution of the distribution of the different subpopulations within the culture stabilized at a stable total biomass concentration.

Two phases could be observed concerning the evolution of fluorescence intensity distribution. First, between 30 and 45 cell generations, fluorescence intensity distribution was maintained at the proportion 20 % P_2, 60 % P_1 and 20 % P_0 (**Figure 6**). At the beginning of the 0.05 h^{-1}-chemostat (*i.e.* between 30 and 33 generations), an increase in the subpopulation P_0 (40 %) was observed to the detriment of the subpopulations P_2 (10 %) and P_1 (50%) (**Figures 5** & **6**), as shown in the boxplots on fluorescence intensity distribution (**Figure 4b**). Over the same time period (*i.e.* 30 to 45 cell generations), P_1–cells decimal reduction rate remained rather low (under 0.20) while it increased transiently for P_2 -cells up to 0.75 (**Figure 7c**). Meanwhile, the decimal reduction rate for kanamycin-resistant cells remained rather low, under 0.20 (**Figure 7d**). Second, between 45 and 55 cell generations, the proportion of the P_2 subpopulation increased from 40 to 60 %, while the proportion of the subpopulations P_0 (5 %) and P_1 (35 %) decreased (**Figure 6**). The fluorescence intensity distribution was centered on the P_2 cell gate with a shoulder in the P_1 cell gate (**Figure 5**; cytogram at 54 generations), and boxplot median ($2 \cdot 10^3$) and mean values ($2.5 \cdot 10^3$) stabilized in FL1-H channel. The overall plasmid-expressing population (eGFP-positive and kanamycin resistant) showed a low decimal reduction rate (**Figures 7 c** & **d**), and the plasmid-based eGFP remained expressed in most cells. This was consistent with the high stable fluorescence intensity distribution in single-cells (**Figure 4b**).

Cell concentration (**Figure 7a**) decreased and stabilized around $7 \cdot 10^8$ cells·mL^{-1} at steady state by flow cytometry. By plate count, cell concentration decreased regularly throughout the cultivation until it reached $1 \cdot 10^9$ cells·mL^{-1} at the end of the first chemostat cultivation.

Therefore, by decreasing the dilution rate to 0.05 h^{-1}, chemostat mode favored the appearance of the subpopulation P_2, which exhibited the highest fluorescence intensity distribution, after 10 numbers of residence time corresponding to 15 generation growing under such condition.

Chemostat at 0.10 h^{-1}

A higher dilution rate of 0.10 h^{-1} was then applied in this experiment. Chemostat was carried out at 37°C and 0.10 h^{-1} for 160 h, corresponding to 23 cell generations (16 hydraulic residence time). As exposed beforehand on macroscopic data, the total biomass concentration was maintained constant at 5 $g_{CDW} \cdot L^{-1}$. Likewise, no significant changes in metabolism were identified based on extracellular metabolites and exhausted gas analyses.

Based on those macroscopic analyses, steady state was reached at 62 generations (7.2 generations after the start of 0.10 h^{-1}-chemostat) and maintained for 23 cell generations.

Between 55 and 62 cell generations (*i.e.* 5 residence times), boxplots showed that the distribution range remained the same width (**Figure 4c**). However, the boxplots themselves were symmetrically transposed by following median / mean increase. This was consistent with the observation, that fluorescence intensity distribution slipped symmetrically through a higher median value in the P_2 cells gate (**Figure 5**) and that the proportion of P_0 and P_1 - cells continued to decline, while the proportion of P_2 cells increased (**Figures 5** & **7a**). Once steady state was reached at 62 generations (*i.e.* 7.2 residence time), boxplots were reproducibly centered on the P_2 - subpopulation (**Figures 4c** & **5**). It was interesting to note that fluorescence intensity distributions median was significantly higher at the end of the 0.10 h^{-1} - chemostat ($1 \cdot 10^4$ in FL1-H) compared to the 0.05 h^{-1} - chemostat ($5 \cdot 10^3$ in FL1-H) (**Figure 4d**) even if they were both mainly included in the P_2 - gate.

On the one hand, the cell concentration measured by flow cytometry increased slightly and stabilized at the steady state at $4 \cdot 10^9$ cells·mL^{-1} (**Figure 7a**). On the other hand, the cell concentration measured by plate count decreased significantly from 1.10^9 to 8.10^7 cells·mL^{-1}. The main reason could lie in the loss of cell cultivability due to the prolonged exposure at 37°C (620 hours from batches to chemostat) and to the higher intracellular eGFP concentration for the P_2 population at 0.10 h^{-1} dilution rate (FL1 median $1 \cdot 10^4$, compared to FL1 median $5 \cdot 10^3$ for P_2 population at 0.05 h^{-1}). Too high, an intracellular concentration of eGFP could indeed be toxic for the cells.

Therefore, increasing the dilution rate from 0.05 to 0.10 h^{-1} favored the maintenance of the P_2 subpopulation compared to P_1 with an increase in the intracellular eGFP concentration for the P_2 population reaching the value of the reference culture at 30°C.

DISCUSSION

Plasmid curing in *Cupriavidus necator* has been used to study the impact of plasmid-encoded mechanisms (*e.g.* hydrogen utilization (Andersen et al., 1981) and toluene metabolism (Hughes et al., 1984)) on both plasmid-bearing and -free cells, by removing the involved plasmid from host cells. Several plasmid curing strategies have been used, presenting with different efficiency levels and ease of use. Here, a plasmid curing method was intended to generate heterogeneity in a cell population in terms of plasmid expression level. Therefore, a mild plasmid curing strategy inducing this heterogeneity was searched without completely inhibiting cell growth.

Temperature increase and rifampicin addition were selected as curing strategies in batch. Despite its lower reported efficiency, rifampicin was chosen as a disruptor of plasmid transcription in bacteria (Buckner et al., 2018) (Wehrli (1983), with the expectation of obtaining an average efficiency on plasmid curing without drastic growth inhibition. Population heterogeneity was studied by flow cytometry based on eGFP-fluorescence and by plate count based on kanamycin resistance.

The heterogeneity was found more pronounced after a temperature increase (30 to 42°C) whereas almost none was observed after rifampicin addition (50 $mg \cdot L^{-1}$). This result confirmed the low efficiency of rifampicin as a curing agent (Buckner et al., 2018).. The plasmid expression level distribution widened after plasmid curing, especially after temperature increase. This expression level heterogeneity at a single-cell level in response to plasmid curing was not observed in previous works, as plasmid stability measurements were mainly based on mean analysis within the overall population (Andersen et al., 1981; Buckner et al., 2018; Hughes et al., 1984; Monchy et al., 2006; Zaman, 2010).

For temperature increase, cell concentrations calculated by plate count were lower than by flow cytometry. For rifampicin addition, there was no difference. Therefore, there was a cultivability loss during plasmid curing by temperature. These observations were supported by propidium iodide staining of cells; after temperature increase, the percentage of permeabilized cells increased up to 15 %, while it remained zero with rifampicin.

Although plate count data presented higher heterogeneity than flow cytometry data (certainly due to cultivability), its level achieved by both counting methods was still quite low. This might be explained by the fact that cell growth drastically slowed down (- 57 %, rifampicin, - 95 %, temperature 42°C) after plasmid curing induction. An insufficient amount of cell generations may have been generated to observe the plasmid curing phenomenon because of the negative impact of both curing agents on cell replication mechanisms.

So, a temperature of 42°C might have been too stringent for cells. Therefore, in the following experiments temperature was set to 37°C instead, allowing inducing heterogeneity and not drastically inhibiting the growth rate.

This was confirmed during successive batches grown at 37°C where a heterogeneity of plasmid expression was still obtained but with a higher growth. The three fluorescent subpopulations P_0 (low / no fluorescence), P_1 (medium fluorescence) and P_2 (high fluorescence), observed in our previous work during successive flasks subcultures (Boy et al., 2020) were observed. Therefore, successive batches at 37°C were proved to be an

effective strategy to obtain a heterogeneous plasmid expression level distribution. The three distinct fluorescent subpopulations P_0, P_1, P_2 were obtained after 30 cell generations. It took way more cell generations to obtain the three distinct subpopulations in successive batches compared to successive flasks subcultures (*i.e.* 19 cell generations (Boy et al. 2020)). This is most probably due to the fact that flask cultures presented more stringent growth conditions that the conditions for bioreactor cultures where the environment was better controlled. (*i.e.* dissolved oxygen concentration and pH).

The continuous cultivation mode is particularly suitable to analyze stress responses of cell subpopulations in a defined physiological state, at a controlled specific growth rate. Here, chemostat was applied to study the impact of the dilution rate on the plasmid expression level by measuring the eGFP fluorescence, under plasmid-curing conditions. This mode of cultivation had already been used in previous works to show that the level of plasmid expression (*i.e.* plasmid replication rate, plasmid copy number) could be regulated by the dilution rate (*i.e.* growth rate) (Dupoet et al., 1987; Klotsky and Schwartz, 1987; Klumpp, 2011; Koizumi et al., 1985; Lin-Chao and Bremer, 1986; Reinikainen and Virkajärvi, 1989; Ryan and Parulekar, 1991). These studies were based on the overall measurement of plasmid DNA content, plasmid copy number, etc. In the literature, different opinions regarding the impact of dilution rate on the level of plasmid expression can be found, as it strongly depends on the "plasmid vector - host cell" association (Chew et al., 1988; D'Angio et al., 1994). For example, different behaviors could be observed depending on the limiting substrate (glucose, ammonium, phosphate or sulphate) or the medium used for the same association (Chew et al., 1988). On the one hand, increased dilution rates led to a decrease in the plasmid copy number. This is the most common trend, as a lower plasmid copy number results in a lower metabolic load and therefore higher growth rate (Patnaik, 2000). This is the case for *Escherichia coli* K12 with plasmid R1 (Light and Molin, 1982), for *E. coli* Br/A with plasmid pBR322 (Lin-Chao and Bremer, 1986) and for *E. coli* JM13 with plasmid pUC8 (Ryan and Parulekar, 1991). On the other hand, plasmids which confer a growth advantage to host cells are less common but might alter the physiological state of cells to favor growth (Patnaik, 2000). It is the case of the association of *E. coli* K12 with the plasmid pBR322 (Klumpp, 2011; Noack et al., 1981; Reinikainen and Virkajärvi, 1989) and also *Bacillus stearothermophilus* CU21 with the plasmid pLP11 (Koizumi et al., 1985), where the plasmid copy number increases with the growth rate. There is not yet a definitive explanation for this phenomenon, but this behavior generally concerns low copy number plasmids and plasmids whose replication is cell-cycle specific (Patnaik, 2000). It has been reported that the plasmid copy number may increase with increasing dilution rates in bacteria, for plasmids with low to medium

copy number. The plasmid used here, pBBR1MCS-2, is known to be a medium copy plasmid at around 30 copies per cell (Buch et al., 2010).

A plasmid curing strategy by raising the temperature was applied in chemostat, hoping to amplify the phenomenon observed in flasks and batch mode, over an increased number of cell generations. The second objective was to analyze the impact of the dilution rate (*i.e.* growth rate). Chemostat was set at 2 dilution rates (0.05 and 0.10 h^{-1}) at 37°C and analyzed in terms of subpopulations. Those dilution rates were chosen because they covered the range of the specific growth rates of the P_1 and P_2 subpopulations previously determined in 96 - well plates in selective medium (Boy et al., 2020). Moreover, 0.05 h^{-1} was close to the lowest specific growth rate observed in the second successive batch at 37°C (where P_2 - cell were still majority). Even when macroscopic steady states were reached after 5 residence times, variations in the fluorescence intensity distribution could be observed. At 0.05 h^{-1}, the steady state favored the settlement of the subpopulation P_1 (80 %) within 10 cell generations, corresponding to 7 residence times. The cell population in the bioreactor was completely renewed and the remaining P_2 - cells from the batches were gradually washed out. However, after 10 new cell generations, a gradual shift was observed towards the increase of the P_2subpopulation. This could be explained by the fact that cells were able to adapt to these conditions of increased temperature for a number of cell generations at this controlled dilution rate. Therefore, at the subpopulation level, the steady state at dilution rate of 0.05 h^{-1} resulted in a 60: 35 % distribution between subpopulations P_2 and P_1, respectively. The fluorescence intensity median reached at the end of the 0.10 h^{-1} - chemostat ($1 \cdot 10^4$ in FL1-H) was significantly higher than that reached at the end of the 0.05 h^{-1} - chemostat ($5 \cdot 10^3$ in FL1-H), even if still was in the P_2 - gate. So, switching the chemostat dilution rate up to 0.10 h^{-1} resulted in the increase of the subpopulation P_2 over the subpopulation P_1. This suggests that the maximal specific growth rates previously estimated for P_1 and P_2 were largely underestimated in 96 - wells plate, otherwise P_2 would have been washed out of the bioreactor. The nearly homogeneous population (90 % P_2) reached at steady state 0.10 h^{-1} could be the result of a growth - rate dependent increase in the plasmid copy number of the P_1 subpopulation to match to the maximal possible number in the strain for this dilution rate (subpopulation P_2). The subpopulation P_2 was maintained and the fluorescence intensity distribution was very stable over time. The cells were able to cope with this higher dilution rate without the need to decrease the protein production performance in supra - optimal temperature conditions, as was also the case under optimal growth conditions.

CONCLUSIONS

Our study showed that well-controlled plasmid curing conditions can be used to generate heterogeneity in plasmid expression in engineered *C. necator* without completely inhibiting cell growth. For this, it was better to use a temperature increase of 30 to 37 °C instead of adding rifampicin. By applying these conditions, to successive batches, we were able to identify three subpopulations with different levels of plasmid-based eGFP expression through the use of our plasmid-encoded eGFP biosensor. The distribution of these three subpopulations could be modulated in chemostat by changing the dilution rate. The further use of the biosensor should make it possible to study the mechanisms underlying the genesis of heterogeneity within the engineered microorganisms cultivated in a bioreactor.

COMPLIANCE WITH ETHICAL STANDARDS

Competing interests

The authors declare that there are no competing interests.

Ethical approval

Not applicable, since the work does not involve any study with human participants or animals

AUTHORS' CONTRIBUTIONS STATEMENT

CB, JL, SA, NG and SG conceived and designed research. CB conducted experiments and analyzed data. CB wrote the manuscript and JL, SA, NG and SG reviewed it. All authors read and approved the manuscript.

DECLARATION

Funding

Funding was obtained from Doctoral Research Assignments from the French Ministry of Research.

Conflicts of interest/Competing interests

The authors declare that there are no competing interests.

Ethics approval

Not applicable, since the work does not involve any study with human participants or animals.

Consent to participate

Not applicable.

Consent for publication

All authors agreed to publish this work.

Availability of data and material

All data generated or analyzed during this study are included in the present work.

Code availability

Not applicable.

REFERENCES

Andersen, K., Tait, R.C., King, W.R., (1981) Plasmids required for utilization of molecular hydrogen by Alcaligenes eutrophus. Archives of Microbiology 129, 384-390. *10.1007/BF00406468*

Aragao, G., (1996) Production de poly-beta-hydroxyalcanoates par Alcaligenes eutrophus: caractérisation cinétique et contribution à l'optimisation de la mise en oeuvre des cultures. Institut National des Sciences Appliquées de Toulouse PHD.

Bazzicalupo, P., Tocchini-Valentini, G.P., (1972) Curing of an Escherichia coli episome by rifampicin (acridine orange-F + -F - -Hfr-lac). Proceedings of the National Academy of Sciences of the United States of America 69, 298-300. *10.1073/pnas.69.2.298*

Binder, D., Drepper, T., Jaeger, K.E., Delvigne, F., Wiechert, W., Kohlheyer, D., Grunberger, A., (2017) Homogenizing bacterial cell factories: Analysis and engineering of phenotypic heterogeneity. Metabolic Engineering 42, 145-156. *10.1016/j.ymben.2017.06.009*

Black, W.B., Zhang, L., Kamoku, C., Liao, J.C., Li, H., (2018) Rearrangement of Coenzyme A-Acylated Carbon Chain Enables Synthesis of Isobutanol via a Novel Pathway in Ralstonia eutropha. ACS Synth Biol 7, 794-800. *10.1021/acssynbio.7b00409*

Boy, C., Lesage, J., Alfenore, S., Gorret, N., Guillouet, S.E., (2020) Plasmid expression level heterogeneity monitoring via heterologous eGFP production at the single-cell level in Cupriavidus necator. Applied Microbiology and Biotechnology. *10.1007/s00253-020-10616-w*

Buch, A.D., Archana, G., Naresh Kumar, G., (2010) Broad-host-range plasmid-mediated metabolic perturbations in Pseudomonas fluorescens 13525. Appl Microbiol Biotechnol 88, 209-218. *10.1007/s00253-010-2717-x*

Buckner, M.M.C., Ciusa, M.L., Piddock, L.J.V., (2018) Strategies to combat antimicrobial resistance: anti-plasmid and plasmid curing. Fems Microbiology Reviews 42, 781-804. *10.1093/femsre/fuy031*

Budde, C.F., Riedel, S.L., Willis, L.B., Rha, C., Sinskey, A.J., (2011) Production of Poly(3-Hydroxybutyrate-co-3-Hydroxyhexanoate) from Plant Oil by Engineered Ralstonia eutropha Strains. Applied and Environmental Microbiology 77, 2847-2854. *10.1128/aem.02429-10*

Carlquist, M., Fernandes, R.L., Helmark, S., Heins, A.L., Lundin, L., Sorensen, S.J., Gernaey, K.V., Lantz, A.E., (2012) Physiological heterogeneities in microbial populations and implications for physical stress tolerance. Microbial Cell Factories 11. *10.1186/1475-2859-11-94*

Chew, L.C.K., Tacon, W.C.A., Cole, J.A., (1988) Effect of growth conditions on the rate of loss of the plasmid pAT153 from continuous cultures of Escherichia coli HB101. Fems Microbiology Letters 56, 101-104. *10.1111/j.1574-6968.1988.tb03157.x*

Crepin, L., Lombard, E., Guillouet, S.E., (2016) Metabolic engineering of Cupriavidus necator for heterotrophic and autotrophic alka(e)ne production. Metabolic Engineering 37, 92-101. *10.1016/j.ymben.2016.05.002*

Cruz, M.V., Gouveia, A.R., Dionísio, M., Freitas, F., Reis, M.A.M., (2019) A Process Engineering Approach to Improve Production of P(3HB) by Cupriavidus necator from Used Cooking Oil. International Journal of Polymer Science 2019, 2191650. *10.1155/2019/2191650*

D'Angio, C., Béal, C., Boquien, C.-Y., Corrieu, G., (1994) Influence of dilution rate and cell immobilization on plasmid stability during continuous cultures of recombinant strains of Lactococcus lactis subsp. lactis. Journal of Biotechnology 34, 87-95. *https://doi.org/10.1016/0168-1656(94)90169-4*

Delvigne, F., Goffin, P., (2014) Microbial heterogeneity affects bioprocess robustness: Dynamic single-cell analysis contributes to understanding of microbial populations. Biotechnology Journal 9, 61-72. *10.1002/biot.201300119*

di Mauro, E., Synder, L., Marino, P., Lamberti, A., Coppo, A., Tocchini-Valentini, G.P., (1969) Rifampicin sensitivity of the components of DNA-dependent RNA polymerase. Nature 222, 533-537. *10.1038/222533a0*

Dupoet, P.D., Arcand, Y., Bernier, R., Barbotin, J.N., Thomas, D., (1987) Plasmid stability in immobilized and free recombinant Escherichia coli JM105(pKK223-200) - Importance of oxygen diffusion, growth rate, and plasmid copy number. Applied and Environmental Microbiology 53, 1548-1555.

Ewering, C., Heuser, F., Benolken, J.K., Bramer, C., Steinbuchel, A., (2006) Metabolic engineering of strains of Ralstonia eutropha and Pseudomonas putida for biotechnological production of 2-methylcitric acid. Metabolic Engineering 8, 587-602. *10.1016/j.ymben.2006.05.007*

Friedrich, C.G., Bowien, B., Friedrich, B., (1979) Formate and oxalate metabolism in Alcaligenes eutrophus. J Gen Microbiol 115, 185-192. *10.1099/00221287-115-1-185*

Fukui, T., Suzuki, M., Tsuge, T., Nakamura, S., (2009) Microbial synthesis of poly((R)-3-hydroxybutyrate-co-3-hydroxypropionate) from unrelated carbon sources by engineered Cupriavidus necator. Biomacromolecules 10, 700-706. *10.1021/bm801391j*

Garrigues, L., Maignien, L., Lombard, E., Singh, J., Guillouet, S.E., (2020) Isopropanol production from carbon dioxide in Cupriavidus necator in a pressurized bioreactor. New Biotechnology 56, 16-20. *https://doi.org/10.1016/j.nbt.2019.11.005*

Gonzalez-Cabaleiro, R., Mitchell, A.M., Smith, W., Wipat, A., Ofiteru, I.D., (2017) Heterogeneity in Pure Microbial Systems: Experimental Measurements and Modeling. Frontiers in Microbiology 8. *10.3389/fmicb.2017.01813*

Grousseau, E., Lu, J.N., Gorret, N., Guillouet, S.E., Sinskey, A.J., (2014) Isopropanol production with engineered Cupriavidus necator as bioproduction platform. Applied Microbiology and Biotechnology 98, 4277-4290. *10.1007/s00253-014-5591-0*

Gruber, S., Hagen, J., Schwab, H., Koefinger, P., (2014) Versatile and stable vectors for efficient gene expression in Ralstonia eutropha H16. Journal of Biotechnology 186, 74-82. *10.1016/j.jbiotec.2014.06.030*

Grunwald, S., Mottet, A., Grousseau, E., Plassmeier, J.K., Popovic, M.K., Uribelarrea, J.L., Gorret, N., Guillouet, S.E., Sinskey, A., (2015) Kinetic and stoichiometric characterization of organoautotrophic growth of Ralstonia eutropha on formic acid in fed-batch and continuous cultures. Microbial Biotechnology 8, 155-163. *10.1111/1751-7915.12149*

Heins, A.L., Weuster-Botz, D., (2018) Population heterogeneity in microbial bioprocesses: origin, analysis, mechanisms, and future perspectives. Bioprocess Biosyst Eng 41, 889-916. *10.1007/s00449-018-1922-3*
Hoefel, T., Wittmann, E., Reinecke, L., Weuster-Botz, D., (2010) Reaction engineering studies for the production of 2-hydroxyisobutyric acid with recombinant Cupriavidus necator H 16. Applied Microbiology and Biotechnology 88, 477-484. *10.1007/s00253-010-2739-4*
Hughes, E.J., Bayly, R.C., Skurray, R.A., (1984) Characterization of a TOL-like plasmid from Alcaligenes eutrophus that controls expression of a chromosomally encoded p-cresol pathway. Journal of bacteriology 158, 73-78.
Johnson, B.F.R.Y.S., (1971) Dissimilation of Aromatic Compounds by Alcaligenes Eutrophus Journal of Bacteriology 107, 468–475.
Klotsky, R.A., Schwartz, I., (1987) Measurement of cat expression from growth-rate-regulated promoters employing beta-lactamase activity as an indicator of plasmid copy number. Gene 55, 141-146. *10.1016/0378-1119(87)90257-5*
Klumpp, S., (2011) Growth-Rate Dependence Reveals Design Principles of Plasmid Copy Number Control. PLOS ONE 6, e20403. *10.1371/journal.pone.0020403*
Koizumi, J., Monden, Y., Aiba, S., (1985) Effects of temperature and dilution rate on the copy number of recombinant plasmid in continuous culture of Bacillus stearothermophilus (pLP11). Biotechnol Bioeng 27, 721-728. *10.1002/bit.260270522*
Koller, M., Atlić, A., Dias, M., Reiterer, A., Braunegg, G., (2010) Microbial PHA Production from Waste Raw Materials. In: Chen, G.G.-Q. (Ed.), Plastics from Bacteria: Natural Functions and Applications. Springer Berlin Heidelberg, Berlin, Heidelberg, pp. 85-119.
Kovach, M.E., Elzer, P.H., Hill, D.S., Robertson, G.T., Farris, M.A., Roop, R.M., Peterson, K.M., (1995) Four new derivatives of the broad-host range cloning vector pBBR1MCS, carrying different antibiotic resistance cassettes. Gene 166, 175-176. *10.1016/0378-1119(95)00584-1*
Krieg, T., Sydow, A., Faust, S., Huth, I., Holtmann, D., (2018) CO(2) to Terpenes: Autotrophic and Electroautotrophic α-Humulene Production with Cupriavidus necator. Angew Chem Int Ed Engl 57, 1879-1882. *10.1002/anie.201711302*
Light, J., Molin, S., (1982) Expression of a copy number control gene (copB) of plasmid R1 is constitutive and growth rate dependent. Journal of Bacteriology 151, 1129-1135.
Lin-Chao, S., Bremer, H., (1986) Effect of the bacterial growth rate on replication control of plasmid pBR322 in Escherichia coli. Molecular and General Genetics MGG 203, 143-149. *10.1007/BF00330395*
Lu, J.N., Brigham, C.J., Rha, C., Sinskey, A.J., (2013) Characterization of an extracellular lipase and its chaperone from Ralstonia eutropha H16. Applied Microbiology and Biotechnology 97, 2443-2454. *10.1007/s00253-012-4115-z*
Marc, J., Grousseau, E., Lombard, E., Sinskey, A.J., Gorret, N., Guillouet, S.E., (2017) Over expression of GroESL in Cupriavidus necator for heterotrophic and autotrophic isopropanol production. Metabolic Engineering 42, 74-84. *10.1016/j.ymben.2017.05.007*
Monchy, S., Benotmane, M.A., Wattiez, R., van Aelst, S., Auquier, V., Borremans, B., Mergeay, M., Taghavi, S., van der Lelie, D., Vallaeys, T., (2006) Transcriptomic and proteomic analyses of the pMOL30-encoded copper resistance in Cupriavidus metallidurans strain CH34. Microbiology-Sgm 152, 1765-1776. *10.1099/mic.0.28593-0*
Muller, J., MacEachran, D., Burd, H., Sathitsuksanoh, N., Bi, C.H., Yeh, Y.C., Lee, T.S., Hillson, N.J., Chhabra, S.R., Singer, S.W., Beller, H.R., (2013) Engineering of Ralstonia eutropha H16 for Autotrophic and Heterotrophic Production of Methyl Ketones. Applied and Environmental Microbiology 79, 4433-4439. *10.1128/aem.00973-13*

Nangle, S.N., Ziesack, M., Buckley, S., Trivedi, D., Loh, D.M., Nocera, D.G., Silver, P.A., (2020) Valorization of CO2; through lithoautotrophic production of sustainable chemicals in Cupriavidus necator. bioRxiv, 2020.2002.2008.940007. *10.1101/2020.02.08.940007*
Noack, D., Roth, M., Geuther, R., Müller, G., Undisz, K., Hoffmeier, C., Gáspár, S., (1981) Maintenance and genetic stability of vector plasmids pBR322 and pBR325 in Escherichia coli K12 strains grown in a chemostat. Molecular and General Genetics MGG 184, 121-124. *10.1007/BF00271207*
Patnaik, P.R., (2000) An evaluation of models for the effect of plasmid copy number on bacterial growth rate. Biotechnology Letters 22, 1719-1725. *10.1023/A:1005696401254*
Pohlmann, A., Fricke, W.F., Reinecke, F., Kusian, B., Liesegang, H., Cramm, R., Eitinger, T., Ewering, C., Potter, M., Schwartz, E., Strittmatter, A., Voss, I., Gottschalk, G., Steinbuchel, A., Friedrich, B., Bowien, B., (2006) Genome sequence of the bioplastic-producing "Knallgas" bacterium Ralstonia eutropha H16. Nature Biotechnology 24, 1257-1262. *10.1038/nbt1244*
Rakotomalala, R., (2011) Tests de normalité - Techniques empiriques et tests statistiques,. Université Lumière Lyon 2 https://docplayer.fr/424798-Tests-de-normalite-techniques-empiriques-et-tests-statistiques.html.
Reinikainen, P., Virkajärvi, I., (1989) Escherichia coli growth and plasmid copy numbers in continuous cultures. Biotechnology Letters 11, 225-230. *10.1007/BF01031568*
Ryan, W., Parulekar, S.J., (1991) Recombinant protein synthesis and plasmid instability in continuous cultures of Escherichia coli JM103 harboring a high copy number plasmid. Biotechnology and Bioengineering 37, 415-429. *10.1002/bit.260370504*
Tang, R., Weng, C., Peng, X., Han, Y., (2020) Metabolic engineering of Cupriavidus necator H16 for improved chemoautotrophic growth and PHB production under oxygen-limiting conditions. Metabolic Engineering 61, 11-23. *https://doi.org/10.1016/j.ymben.2020.04.009*
Trevors, J.T., (1986) Plasmid curing in bacteria. Fems Microbiology Letters 32, 149-157.
Wehrli, W., (1983) Rifampin: Mechanisms of Action and Resistance. Reviews of Infectious Diseases 5, S407-S411. *10.1093/clinids/5.Supplement_3.S407*
Zaman, M.P., MH.; Akhter MZ., (2010) Plasmid Curing of Escherichia coli Cells with Ethidium Bromide, Sodium, Dodecyl Sulfate and Acridine Orange. Bangladesh Journal of Microbiology 27, 28-31.

LEGEND OF THE FIGURES

Figure 1: Box plot representation of fluorescence intensity distribution of eGFP-positive cells in the FL1-A channel throughout fermentation for the strain Re2133/pCB1 under plasmid curing conditions with rifampicin addition (time (a) and generations (b)) and temperature increase (time (c), generations (d) and magnification between 6 and 7.5 generations (e)).

Figure 2: Cell concentration in cells·L^{-1} for the rifampicin experiment, vs cell generations by plate count (◆ Gen^R and ◆ Gen^R+Kan^R) and flow cytometry (● Single cells and ● eGFP-positive cells) (**a**). Cell concentration in cells·L^{-1} for the temperature experiment, vs cell generations by plate count (◆ Gen^R and ◆ Gen^R+Kan^R) and flow cytometry (● Single cells and ● eGFP-positive cells) (**b**). Decimal reduction rate for the rifampicin (**c**) and temperature (**d**) experiments, vs cell generations by plate count (◆) and flow cytometry (●).

Figure 3: Comparison of extracellular fluorescence intensity and the percentage of permeabilized cells throughout fermentation with addition of rifampicin (**a**) and temperature increase at 37°C (**b**). Legend: (●) % PI-positive cells; (■) extracellular fluorescence intensity.

Figure 4: Plasmid expression levels represented through fluorescence intensity distribution in the FL1-H channel by boxplots during successive batches at 30 and 37°C (**a**), chemostat at 37°C and 0.05 h^{-1} (**b**) and chemostat at 37°C and 0.10 h^{-1} (**c**). Comparison of plasmid expression level distribution on the last point of the 0.05 and 0.1 h^{-1} chemostats, at respectively, 53 and 75 generations (**d**). Delimitation between successive batches were shown by blue and grey vertical lines.

Figure 5: Evolution of fluorescence intensity distribution in the FL1-H channel at different time of culture.

Figure 6: Percentage of P_2-cells (■) and P_1-cells (■) and P_0-cells (■) by flow cytometry through the number of cell generations, and the number of residence time. Red vertical lines represent the delimitation between fermentation conducts (batch, chemostat).

Figure 7: Cell concentrations vs the number of generations for (**a**) fluorescent cells (●) and total cells (✚) determined by flow cytometry as well as (**b**) Gen^R cells (●) and Gen^RKan^R cells (◆). (**c**) Decimal reduction rate vs the number of generations for P_2-cells (■), P_1-cells (▲), P_0-cells (▼) and for (**d**) Gen^RKan^R cells (●).

TITLE

Study of plasmid-based expression level heterogeneity under plasmid-curing like conditions in *Cupriavidus necator*

AUTHORS

Catherine BOY[1], Julie LESAGE[1], Sandrine ALFENORE[1], Stéphane E. GUILLOUET[1], Nathalie GORRET[1*],

[1] TBI, Université de Toulouse, CNRS, INRA, INSA, Toulouse, France

*CORRESPONDING AUTHOR

Nathalie GORRET

ngorret@insa-toulouse.fr

TBI, Université de Toulouse, CNRS, INRA, INSA, Toulouse, France

135 Avenue de Rangueil – 31077 Toulouse Cedex 04

ABSTRACT

Plasmid expression level heterogeneity in *Cupriavidus necator* was studied in response to stringent culture conditions, supposed to enhance plasmid instability, through plasmid curing strategies. Two plasmid curing strategies were compared based on their efficiency at generating heterogeneity in batch: rifampicin addition and temperature increase. A temperature increase from 30 to 37°C was the most efficient plasmid curing strategy. To generate a heterogeneous population in terms of plasmid expression levels, successive batches at supra-optimal culture temperature (*i.e.* 37°C) were initially conducted. Three distinct fluorescent subpopulations P_0 (not fluorescent), P_1 (low fluorescence intensity, median = 1 10^3) and P_2 (high fluorescence intensity, median = 6 10^3) were obtained. From there, the chemostat culture was implemented to study the long-term stress response under well-controlled environment at defined dilution rates. For dilution rates comprised between 0.05 and 0.10 h^{-1}, the subpopulation P_2 (62 % *vs* 90 %) was favored compared to P_1 cells (54 % *vs* 1 %), especially when growth rate increased. Our biosensor was efficient at discriminating subpopulation presenting different expression levels under stringent culture conditions. Plus, we showed that controlling growth kinetics had a stabilizing impact on plasmid expression levels, even under heterogeneous expression conditions.

KEYWORDS:

Plasmid curing, chemostat, plasmid stability, expression level, flow cytometry, Single-cell analysis

INTRODUCTION

Historically, microbial populations cultivated in assumed homogeneous environments are by extension also considered homogeneous in terms of its individuals. Nowadays, this postulate is being discussed and more and more studies showing that population heterogeneity can be observed among monoclonal cultures in homogeneous environments are being published (Carlquist et al., 2012; Delvigne and Goffin, 2014; Gonzalez-Cabaleiro et al., 2017; Heins and Weuster-Botz, 2018). In recombinant bioprocesses, population heterogeneity contributes to enhance process instability (Binder et al., 2017). Therefore, a better understanding of the mechanisms leading to phenotypic homogeneity of engineered strains is mandatory to ensure bioprocess robustness. In previous work (Boy et *al.*, 2020), a plasmid expression level monitoring method based on the expression of a plasmid-encoded eGFP biosensor has been designed, in order to identify subpopulations presenting different phenotypic behaviors. Its single-cell response to artificially induce plasmid expression level heterogeneity was studied in flasks through cell sorting through FACS (*i.e.* Fluorescence Activated Cell Sorting) technology. FACS allows the physiological characteristics of each subpopulation to be studied separately (*i.e.* growth rate) (Boy et al., 2020). As these experiments were performed in flasks with less than 20 cell generations, it would be interesting to increase the cell generation number submitted to plasmid curing-like conditions to amplify the heterogeneity in plasmid expression levels. In this work, the response of our plasmid expression level monitoring method in plasmid curing-like conditions is studied.

Plasmid curing strategies are developed to favor the removal of plasmids from bacterial cells, generally to obtain plasmid-free cells to study specific plasmid-encoded metabolisms (Andersen et al., 1981; Hughes et al., 1984; Monchy et al., 2006); or as a strategy to combat plasmid encoded antimicrobial resistance (Buckner et al., 2018; Zaman, 2010). The choice of the most appropriate curing agent for a plasmid vector is difficult to predict. Plasmids differ significantly in their ability to be cured based on their own properties. Thus, no universally effective curative agent has yet been identified. . (Trevors, 1986; Zaman, 2010). Many strategies have been developed over the years and are generally based on temperature increase (Andersen et al., 1981; Buckner et al., 2018; Hughes et al., 1984), plasmid incompatibility (Buckner et al., 2018; Trevors, 1986), antibiotic addition (*such as*. mitomycin C (Andersen et al., 1981; Hughes et al., 1984; Trevors, 1986), novobiocin (Trevors, 1986), rifampicin (Andersen et al., 1981; di Mauro et al., 1969; Hughes et al., 1984; Trevors, 1986)), addition of DNA

intercalating agents (*such as.* acridine orange (Andersen et al., 1981; Zaman, 2010)), acriflavine (Trevors, 1986), ethidium bromide (Andersen et al., 1981; Zaman, 2010)), or detergent additions (*such as.* sodium dodecyl sulphate (Andersen et al., 1981; Zaman, 2010)). In most protocols, plasmid curing techniques are coupled with successive subcultures under these stringent conditions. *Cupriavidus sp.* homologous plasmids have already been removed by some of these methods: acridine orange, ethidium bromide, sodium dodecyl sulfate (Andersen et al., 1981), benzoate (Hughes et al., 1984), rifampicin, mitomycin C and higher growth temperature (Andersen et al., 1981; Hughes et al., 1984). In this work, attention was drawn to rifampicin addition and temperature increase.

Rifampicin addition as plasmid curing strategy was interesting in our case of study, as it causes variations in the plasmid expression level through disruption in DNA transcription. Rifampicin was shown to bind and consequently to inhibit RNA polymerase molecule, the enzyme responsible for DNA transcription by forming a stable drug-enzyme complex (Wehrli, 1983). In Bazzicalupo et *al.* (1972), rifampicin specifically inhibited the initiation step in the reaction catalyzed by RNA polymerase, therefore eliminating the F'-lac plasmid from *E. coli*. Studies showed that plasmids seemed to have been completely cured from *Escherichia coli* (Haemolysin and F'-lac plasmids (Buckner et al., 2018)), *Staphylococcus aureus* (Penicillinase plasmids (Buckner et al., 2018; Trevors, 1986)) and *Cupriavidus necator* (100 $mg \cdot L^{-1}$ for Hydrogenase plasmids (Andersen et al., 1981)). Nevertheless, rifampicin did not allow curing plasmid from *E. coli* strains whose RNA polymerases were rifampicin-resistant (Bazzicalupo and Tocchini-Valentini, 1972; Buckner et al., 2018; di Mauro et al., 1969; Trevors, 1986).

Increasing growth temperature from 5 to 7°C above the optimal growth temperature was used as an effective curing strategy. The mechanisms of thermal curing of plasmids are not well known. Hypotheses suggest that the application of temperatures above the optimum operating temperature of RNA polymerases could directly interfere with plasmid replication mechanisms. This curing strategy was coupled with series of subcultures using successive inoculations when log phase has been reached (Trevors, 1986). Several cell generations have to be generated in order to be efficient. In *C. necator*, a growth temperature of 42°C (12 degree above optimal growth temperature) was successfully applied for curing plasmids (Hughes et al., 1984).

Cupriavidus necator has regained much interest in recent years, due to its natural metabolic potentialities such as both autotrophic and heterotrophic growth (Budde et al., 2011; Crepin et al., 2016; Friedrich et al., 1979; Grousseau et al., 2014; Grunwald et al., 2015; Johnson, 1971; Marc et al., 2017), and as its poly-β-hydroxybutyrate (PHB) biosynthesis pathways (Cruz et al., 2019; Koller et al., 2010; Nangle et al., 2020;

Pohlmann et al., 2006; Tang et al., 2020). Especially, synthetic biology and metabolic engineering have been implemented in order to build heterologous metabolic pathways for synthon biosynthesis (Black et al., 2018; Crepin et al., 2016; Ewering et al., 2006; Garrigues et al., 2020; Grousseau et al., 2014; Hoefel et al., 2010; Krieg et al., 2018; Marc et al., 2017; Muller et al., 2013). In that context, it is crucial to develop and validate tools to be able to evaluate the robustness of strain within a bioprocess.

In order to further evaluate our capacity to monitor the heterogeneity of plasmid expression level at the single-cell level, *C. necator* strains bearing an engineered eGFP-biosensor plasmid were submitted to two plasmid curing conditions (temperature increase and rifampicin addition) to artificially induce heterogeneity. Herein we aimed at studying more precisely the response of the biosensor under various cultivation modes (batch and chemostat) and investigating the impact of growth rate on plasmid expression level heterogeneity. First, the two plasmid curing strategies were led in batch mode to evaluate their impact on cell physiology (subpopulations) and cell macroscopic behavior. Then, the most efficient plasmid curing strategy was applied in chemostat.

MATERIAL AND METHODS

Strain, plasmids and media

Strains

C. necator Re2133 (Budde et al., 2011) was chosen as expression strain. It was derived from the wildtype strain *C. necator* H16 / ATCC17699 whose genes encoding for acetoacetyl-CoA reductases (*phaB1B2B3*) and for PHA synthase (*phaC1*) were deleted. *Cupriavidus necator* is naturally resistant to gentamicin. Plasmid constructions were achieved through the strains *Escherichia coli* S17-1 (ATCC 47055) and Top10 (InvitrogenTM, Life technologies).

Plasmids

The plasmid CB1 was used in this work. This plasmid encodes for an eGFP through the insertion of the P_{lac}-*egfp* cassette (Gruber et al., 2014) on the pBBad (Fukui et al., 2009) backbone, derived from the pBBR1MCS-2 plasmid (Kovach et al., 1995), which bears kanamycin resistance (Kan^R). Its design and associated molecular biology protocols were described in more details in Boy et *al*. (2020).

Media

The rich medium used for precultures was Tryptic Soy Broth (TSB, 27.5 $g \cdot L^{-1}$, Becton Dickinson, Sparks, MD, USA). Gentamicin (10 $mg \cdot L^{-1}$) and kanamycin (200 $mg \cdot L^{-1}$) were added as final concentrations to ensure purity of the culture and plasmid stability, respectively. To prepare Tryptic Soy Agar (*abbr.* TSA) plates, TSB medium was supplemented with 20 $g \cdot L^{-1}$ agar.

For molecular biology, the rich Lysogeny broth medium (*abbr.* LB) was used (10 $g \cdot L^{-1}$ peptone, 5 $g \cdot L^{-1}$ yeast extract, 10 $g \cdot L^{-1}$ NaCl). Same as above, LB medium was supplemented with 20 $g \cdot L^{-1}$ agar to produce LB agar plates.

The mineral medium for flasks cultivation was detailed in Lu et *al.* (Lu et al., 2013). Gentamicin (10 $mg \cdot L^{-1}$) and kanamycin (200 $mg \cdot L^{-1}$) were added to this medium. The carbon and nitrogen sources used were respectively fructose (20 $g \cdot L^{-1}$) and NH_4Cl (0.5 $g \cdot L^{-1}$).

The mineral medium used for bioreactor cultivation was composed as follows (per liter): $(NH_4)_2SO_4$, 2.8 g; $MgSO_4$-$7H_2O$, 0.75 g; rich phosphorus solution (Na_2HPO_4-$12H_2O$, 1.50 g; KH_2PO_4, 0.25 g); nitrilotriacetic acid, 0.285 g; ammonium iron(III) citrate (28%), 0.090 g; $CaCl_2$, 0.015 g; trace elements (H_3BO_3, 0.45 mg; $CoCl_2$-$6H_2O$, 0.30 mg; $ZnSO_4$,$7H_2O$, 0.15 mg; $MnCl_2$-$4H_2O$, 0.045 mg; Na_2MoO4-$2H_2O$, 0.045 mg; $NiCl_2$-$6H_2O$, 0.03 mg; $CuSO_4$, 0.015 mg). Fructose (30 $g \cdot L^{-1}$) was used as carbon source.

Inoculum Preparation

Inoculum preparation was performed exactly as described in Boy et *al.* (2020).

Plasmid curing during batch cultivations on fructose

Batch cultivations in multi-instrumented 5 L bioreactor Biostat®B-DCU (Sartorius, Germany) were carried out as described in Boy et *al.* (2020). Temperature (30 - 42°C), pH (7) and partial pressure of dioxygen (pO2 > 30 %) in the medium could be controlled throughout culture.

Initial fructose concentration in medium was 50 $g \cdot L^{-1}$ and pulses of both rich phosphorus solution (7 $mL \cdot L^{-1}$) and trace elements solution (2 $mL \cdot L^{-1}$) were performed every 10 $g \cdot L^{-1}$ of biomass produced to prevent nutrient depletion.

After reaching a concentration of 7.5 $g_{CDW} \cdot L^{-1}$ of biomass in the bioreactor, plasmid curing strategies were applied: either by an addition of 50 $mg \cdot L^{-1}$ of rifampicin or an increase of the temperature of culture up to 42°C.

Successive batch subcultures from 30 to 37°C

To generate population heterogeneity prior the start of the continuous culture, successive batch subcultures were made. Batch cultivations were performed as detailed above with an initial fructose concentration of 10 $g \cdot L^{-1}$. The first batch was carried out at 30°C until fructose was completely consumed, 900 mL fermentation broth was then withdrawn through a peristaltic pump and 900 mL of fresh bioreactor mineral medium were added in the bioreactor. Temperature was increased at 37°C. For the seven next batches at 37°C, the protocol was the same. After the eighth batch at 37°C, the chemostat cultivation was started.

Plasmid curing during continuous cultivation on fructose

Fructose-limited continuous culture was established by feeding the bioreactor with fresh medium (Bioreactor mineral medium supplemented with 10 $g \cdot L^{-1}$ fructose). In chemostat-modes, 2 dilution rates were investigated at 0.05 and 0.10 h^{-1} respectively.

Steady state conditions were reached after at least five residence times (*i.e.* 0.05 h^{-1}, 100 h and 7.21 cell generations; 0.10 h^{-1}, 50 h and 7.21 cell generations). The steady state phase was assessed through constant measurements of biomass and residual fructose concentrations, as well as stable composition of the exhaust gases. Temperature was set at 37°C, and pH was regulated at 7. The partial pressure of dioxygen was maintained at 30 % of the saturation through aeration and stirring regulation.

Analytical procedure

Biomass characterization

Biomass concentration was measured by optical density (OD) at 600 nm using a visible spectrophotometer (DR3900, Hachlange, Loveland, Colorado, USA) with a 0.2 cm path length absorption cell (Hellma). OD was correlated to cell dry weight (CDW) measurements (*i.e.* 2 $g_{CDW} \cdot L^{-1}$ = 1 OD unit). For cell dry weight measurements, 0.2 µm pore-size polyamide membranes (Sartorius, Göttingen, Germany), were beforehand dried (60°C, 200mmHg, 72 h) and weighted. Culture medium was sampled and filtrated on dried membranes which were dried again in the same conditions.

Metabolite quantification

Cells samples were centrifuged, and supernatants were filtrated (0.2 µm PTFE syringe filters, VWR) before being used for substrate and products determination. The residual fructose concentration was quantified by high-performance liquid chromatography (HPLC). Other metabolites were searched using the same protocol and calibration curve were set for acetic, formic, propionic, pyruvic succinic acids. The HPLC instrument (Series 1100, Agilent) was equipped with an ion-exchange column (Aminex HPX-87H, 300×7.8 mm, Bio-Rad, Hercules, CA, USA) protected with a guard column (Cation H+ cartridge, 30×4.6 mm, Bio-Rad) and coupled to a RI detector and an UV detector (λ=210 nm). The column was eluted with 2.5 mM H_2SO_4 as a mobile phase at 50 °C at a flow rate of 0.5 mL·min^{-1}. Residual nitrogen was quantified by higher-pressure ionic chromatography (HPIC). The HPIC instrument (ICS-2100 RFIC, Dionex) was equipped with an IonPac™ CS16 column (RFIC™, 3x50mm, BioRad) and an ion suppressor CERS 500 (2 mm, Thermo Scientific). The column was eluted with 30 mM methanesulfonic acid as a mobile phase at 40 °C and a 40 mA ion suppressor current, at a flow rate of 0.36 mL·min^{-1}.

Plate count

C. necator is naturally resistant to gentamycin and plasmid-bearing cells are resistant to kanamycin. Plasmid stability was quantified by parallel plate count on antibiotic selective TSB Petri dishes (10 mg·L^{-1} Gentamicin and 10 mg·L^{-1} Gentamicin + 200 mg·L^{-1} Kanamycin). Serial dilutions were performed in physiological water (0.85 % NaCl) tubes (BioMérieux, Marcy-l'Étoile, France). For every sample, three dilutions were tested, between 10^{-5} and 10^{-9}. The diluted samples were plated in triplicate with the Whitley Automated Spiral Plater (Don Whitley Scientific, Shipley, UK). The results of cell plate counting method were reproducible within 10% based on 3 dilutions in triplicate.

From these data, the decimal reduction rate of plasmid-expressing cells was calculated as the ratio of the concentration of total cells (Gen^R) on the concentration of plasmid-expressing cells (Gen^RKan^R); this ratio was converted to logarithm.

Flow cytometry

Cell permeability (FL3 fluorescence channel) and eGFP-fluorescence (FL1 fluorescence channel) were measured at single-cell level with the BD Accuri C6® flow cytometer (BD Biosciences, Franklin Lakes, NJ, USA). Samples were diluted in physiological water to 10^6 cells mL^{-1}. Samples were run until 20, 000 events were counted at 14 µL·min^{-1} using milli-Q water as sheath fluid. The Forward Scatter Signal (threshold: 12,

000) and Side Scatter Signal (threshold: 2, 000) were used as trigger channels. Data acquisition was performed with BD Accuri CFlow® software. Data processing was achieved with FlowJo software (Becton Dickinson, Sparks, MD, USA). Events consider as *C. necator* cells (total cells) were gated based on a double-singlet gating method, selecting only cells situated on the bisectors of both the (FSC-A vs. FSC-H) and (SSC-A vs. SSC-H).

For the quantification of permeable cells, propidium iodide (PI) (Molecular probes, Invitrogen, USA) was used. After dilution, cell samples were stained with 20 µL of the commercial solution at 1 $mg \cdot L^{-1}$ PI and incubated 20 minutes at room temperature in the dark. A 100 % dead–cell control (100% permeable cells) was prepared by incubating cells in 70 % isopropanol for 1 h at room temperature. The % of permeabilized cells was determined as being the ratio between the number of PI labelled cells and of total cells.

For the analysis of the distribution of eGFP-fluorescence cells, fluorescence intensity was measured at single-cell level on the FL1 fluorescent channel. Decimal reduction rate was calculated as described above from plasmid-expressing cells (eGFP-positive cells; FL1-A > $8 \cdot 10^2$) and total cells. The eGFP-subpopulations P0, P1, P2 were defined based on (FL1-A) fluorescence intensity distribution within the total cells as the one described in Boy et al., 2020.

Extracellular fluorescence measurement

Samples were centrifuged 3 min at 13, 000 rpm with a MiniSpin® table-top microcentrifuge (Eppendorf, Germany) to remove cells from the liquid. The extracellular fluorescence intensity in the supernatant was measured with the Synergy™ HT (Biotek®, USA) multiplate reader at excitation wavelength 485 ± 20 nm and emission wavelength 525 ± 20 nm at sensitivity of 50. Black Nunclon® 96-well plates (ThermoFisher, USA) were used.

Statistical analysis: Normality of distribution functions by BoxPlot representation

The boxplot method aims at representing data distribution through the graphical depiction of its main statistical features, such as the median (50^{th} percentile), the first (25^{th} percentile) and third quartiles (75^{th} percentile). The first and third quartiles correspond to the bottom and top of the boxplot, respectively. The line inside the boxplot symbolizes the median. The interquartile range (*abbr.* IQR) between the first and third quartiles represents the length of the boxplot. The whiskers symbolize the minimum and maximum values as long as they are located within 1.5 x IQR from both extremities of the box. Above 1.5 x IQR, outliers are represented by points (Boy et

al., 2020). A symmetric boxplot centered on the median is commonly considered as normally distributed (Rakotomalala, 2011).

Data analysis

The error on the specific growth rate (determined as being the slope of $\ln[g_{CDW} \cdot L^{-1}] = f(t)$ for batch on dry mass) was calculated as the standard deviation (SD) of the slope. For the yield determination, the state variables (concentrations for batch or weights for fed-batch) were plotted pairwise in a scatter plot within the considered period of the culture. A linear regression was applied to determine the yield (as the slope) and the error (as the SD of the slope).

RESULTS

In order to evaluate our capacity to monitor heterogeneity in plasmid expression level at the single-cell level, the *C. necator* strain Re2133 was transformed with the biosensor-encoding plasmid (pCB1) (Boy et al., 2020). Cell population was analyzed by flow cytometry throughout the cultivation in order to get access to single-cells analysis. Therefore, the distribution of plasmid expression levels could be analyzed in relation to fluorescence intensity distribution within the entire population. As it was previously demonstrated that the plasmid pCB1 presented a low metabolic burden on *C. necator* Re2133 host cells (Boy et al., 2020), any variations detected in the plasmid expression could be attributed to external factors, like plasmid curing strategy, or variations in dilution rate.

Plasmid curing strategy suitable with expression level monitoring during batch cultures

Two different plasmid curing strategies, temperature increase and rifampicin addition, were carried out in batch mode with the strain Re2133/pCB1 in order to define the most efficient method to enhance heterogeneity in plasmid expression. Analyses were supported by macroscopic data (*e.g.* growth kinetics, yields) and population heterogeneity description.

Impact of rifampicin addition and temperature increase on the growth of C. necator Re2133/pCB1 in batch

For the rifampicin-based strategy, preliminary cultures in flasks were achieved beforehand in order to evaluate the concentration of rifampicin needed in the bioreactor to induce plasmid curing (*data not shown*), concentrations from 50 to 150 $mg \cdot L^{-1}$ were tested. A concentration of 50 $mg \cdot L^{-1}$ rifampicin allowed the highest

reduction in the number of plasmid-expressing cells without completely inhibiting growth. For the temperature-based strategy, temperature regulation was set at 42°C, based on previous experiments described in the literature (Andersen et al., 1981; Trevors, 1986).

For both strategies, cultivations in bioreactors were achieved under optimal culture conditions up to 7.5 $g_{CDW} \cdot L^{-1}$ of biomass in the bioreactor. Then, plasmid curing was induced in both bioreactors.

The specific growth rates during the different phases were determined from the biomass concentration evolution (**Table 1**). After rifampicin addition, the specific growth rate dropped to 0.09 ± 0.01 h^{-1}. After temperature increase, growth rate was drastically reduced to 0.009 ± 0.001 h^{-1}. Once biomass reached a concentration of 10 $g_{CDW} \cdot L^{-1}$ (6.6 cell generations), temperature was set back at 30°C to verify the reversibility of the phenomenon. Growth rate remained greatly diminished and only reached 0.04 ± 0.01 h^{-1} after 13 h (about 1 generation).

Biomass production yields (**Table 1**) were evaluated from fructose consumption concentrations and compared to theoretical data 0.53 $g.g^{-1}$ (Aragao, 1996). As expected, before plasmid curing induction, the overall biomass production yields were comparable for both cultures, within 0.47 ± 0.02 $g_X \cdot g_S^{-1}$, and rather close to the theoretical yield. However, after plasmid curing induction, yield values decreased for both strategies. The reduction rate was more important after temperature increase (-62%) than after rifampicin addition (-27%). After switching temperature back to 30°C, yield seemed to be recovered close to the theoretical reference value, even when the growth rate was still affected.

Subpopulation characterization

Plasmid expression level monitoring

The fluorescence intensity distribution of eGFP fluorescent cells was measured by flow cytometry in order to quantify different expression levels. Boxplots have been chosen to represent fluorescence intensity distributions. Distributions of population are represented versus both the generation number and the time course of the culture. Data were presented according to cell generations, in order to compare experiments regardless of growth dynamics and to highlight the number of time cells were divided instead of the duration of the experimentations.

Under optimal culture conditions, fluorescence intensity distribution was Gaussian for both cultures, as the first and third quartiles had equal lengths, and as the mean and median values were equal (**Figure 1**). Plasmid curing conditions were induced after 5.9 generations. For plasmid curing by rifampicin addition (**Figures 1a** & **b**), the

first quartile widened showing a slight sliding of the fluorescence intensity distribution toward lesser fluorescent cells. For plasmid curing by temperature increase at 42°C (**Figures 1c** & **d**), fluorescence intensity distribution widened globally and the median slipped toward lower fluorescence intensity distribution. This phenomenon seemed to be partly reversible as median increased again when temperature was set back to 30°C. This was not due to a change in the quantum yield of eGFP at 42°C and 30°C, as it was verified that eGFP was not impacted by temperature increase at 42°C. To do this, supernatant samples were incubated at 42°C for 24 h, and no variation in the value of fluorescence intensity was detected compared to 37°C (*data not shown*). For an equal generation number between both plasmid curing conditions, the associated culture length is way longer for temperature increase (70 h), as growth rate was highly diminished, compared to rifampicin addition (25 h).

Plasmid stability

Plasmid expression stability was evaluated through flow cytometry and plate count. A gap in cell concentrations between plate count and flow cytometry might reveal a cultivability loss, due to the side effects of plasmid curing on the physiology of host cells. In addition, the dynamic of plasmid expression was evaluated through decimal reduction rates.

In the rifampicin experiment (**Figure 2a**), concentrations of total cells and of cells expressing the plasmid were consistent both by plate count and flow cytometry throughout the culture; meaning gentamicin resistant cell concentration (Gen^R) was equal to single-cell concentration, and that gentamicin and kanamycin resistant cell concentration (Gen^RKan^R) was equal to eGFP-positive cell concentration. The cultivability was not reduced by rifampicin addition. The specific growth rate calculated from the single-cells concentration by flow cytometry was compared to the one determined from the cell dry weight, described beforehand. Growth rate by flow cytometry was evaluated at 0.24 ± 0.03 h^{-1} under optimal growth conditions, and at 0.06 ± 0.05 h^{-1} after plasmid curing induction. Even if growth rate evaluation was noisier by flow cytometry, the orders of magnitude reached was once again equivalent. Thus, flow cytometry and cell dry weight measurements gave comparable growth dynamics. The decimal reduction rate (**Figure 2c**) remained lower than 0.05 for both counting methods confirming that there was no significant decrease in the plasmid expression due to rifampicin addition.

In the temperature experiment (**Figure 2b**), total and plasmid-expressing cell concentrations were consistent both by plate count and flow cytometry under optimal growth conditions. After plasmid curing induction, the gap between the two counting methods increased reaching a one-decade difference for both plasmid-expressing cell and total cell populations. Growth considerably slowed down and cell concentration even decreased for both

Gen^R and Gen^RKan^R populations, which might confirm that cell cultivability decreased at 42°C. When temperature was set back to 30°C after 6.6 cell generations, cell concentration increased slightly for both counting methods and both cell populations. Returning to optimal temperature conditions has prevented further decrease in cell cultivability, but did not allow a complete recovery of cells, as they were not able to grow at their original rate. Like for rifampicin, the growth rate from flow cytometry was compared to growth rate from cell dry weight. Growth rate by flow cytometry was evaluated at 0.23 ± 0.04 h^{-1} under optimal growth conditions, at 0.004 ± 0.004 h^{-1} after plasmid curing induction and at 0.03 ± 0.05 h^{-1} after temperature was set back to 30°C, consistent with the ones calculated from biomass.

Decimal reduction rate (**Figure 2d**) reached a maximum value of 0.18 for plasmid curing by temperature increase and 0.06 by rifampicin. Batch conditions were identical as both precultures were led exactly in the same manner; permeability as well as fluorescence levels were also verified to be identical before bioreactor inoculation. A low decimal reduction rate was measured before plasmid curing induction, either by temperature or rifampicin, by both counting methods: flow cytometry and plate count. After thermal plasmid curing induction, decimal reduction rate increased from 0 to 0.16 by flow cytometry, and from 0.04 to 0.15 by plate count. This value stabilized around 0.18 by both counting methods after temperature decrease. No significant increase was detected after rifampicin addition, by both counting methods.

Plasmid expression loss increased significantly after plasmid curing induction. When comparing plasmid curing strategies, it appears obvious that temperature increase presented the most negative effect on the cell concentration for plasmid-expressing and total cell populations, and consequently on the decimal reduction rate. This negative impact was more notable on plate count measurements, certainly due to cultivability loss.

Cell permeability and eGFP leakage

To further investigate cell physiology, cell permeability and eGFP leakage in the medium were investigated (**Figure 3**). Under optimal culture conditions, the percentage of permeabilized cells was low (% PI - positive cells < 5 %) for both experiments. The higher RFU value at the beginning of the batches might be due to a higher eGFP leakage in flasks precultures. Relative extracellular fluorescence intensity (*i.e.* extracellular fluorescence intensity normalized by optical density at 600 nm) decreased, because optical density increased significantly faster than extracellular fluorescence intensity. This was consistent with low cell permeabilization **(Figure 3)** and the stable normal fluorescence intensity distribution showed above (**Figure 1**). Therefore, eGFP

excretion in the medium was low under optimum culture conditions. Initial optical density and fluorescence intensity in the supernatant were taken as reference to calculate relative fluorescence intensity in the medium.

After rifampicin addition (**Figure 3a**), the percentage of permeabilized cells remained low. The relative extracellular fluorescence intensity was constant, meaning that the amount eGFP excreted by cells became constant and stable.

After temperature increase (**Figure 3b**), the percentage of permeabilized cells increased quickly up to 10 %. The relative extracellular fluorescence intensity increased abruptly. Since cell growth had stopped, the increase in relative extracellular fluorescence was only due to enhanced cell permeabilization. As a result, the fluorescence intensity distribution decreased in single-cells (**Figure 1**). Thus, single-cells excreted more eGFP as the percentage of permeabilized cells increased. When temperature was set back to 30°C, cell permeabilization percentage decreased, because the newly formed cell population was not permeable and so, overthrown the cell population permeabilized by temperature. Meanwhile, relative extracellular fluorescence intensity decreased. Temperature increase led to an enhanced eGFP leakage outside of cells, but this phenomenon could be slowed down by returning to optimal temperature.

The most appropriate approach to generate population heterogeneity had to be selected for further experiments. Plasmid curing by temperature led to a significant decrease in the plasmid expression levels (increase of decimal reduction rate), which was not the case with rifampicin addition. It might be partially due to too stringent culture conditions as shown by high cell permeabilization percentage and cultivability loss by plate count. Both strategies led to decreased growth rate. However, temperature increase at 42°C almost completely inhibited growth. Therefore, temperature increase was the most promising method to induce population heterogeneity. However, to avoid too high cell permeabilization and cultivability loss, the setpoint temperature for the following experiments had to be slightly decreased at 37°C.

Plasmid expression level monitoring during continuous culture at supra-optimal temperature

In order to study the impact of the dilution rate (*i.e.* growth rate) on the stability of the plasmid expression, eGFP fluorescence was measured in cells cultivated in chemostat under fructose limitation and under plasmid-curing conditions (i.e. temperature increase). It has been reported that the plasmid replication rate and / or plasmid copy number could be regulated by the dilution rate in chemostat (Klumpp, 2011; Koizumi et al., 1985; Reinikainen and Virkajärvi, 1989).

The combination of plasmid curing and chemostat mode should make it possible to create more cell generations (hopefully to amplify the phenomenon observed in batch mode) and to study the impact of the dilution rate (*i.e.* growth rate) on plasmid stability.

As mentioned above, the chemostat temperature was set at 37°C instead of 42°C, representing a 7°C - increase from the optimal temperature, which was advised for plasmid-curing experiments (Trevors, 1986). This temperature condition had already been applied in our previous work for plasmid curing during successive subcultures in flasks (Boy et al., 2020). In such condition, three different subpopulations were discriminated based on their fluorescence intensity distribution after 19 cell generations: P_0 (no fluorescence), P_1 (low fluorescence intensity, median value in FL1-H = $1 \cdot 10^3$) and P_2 (high fluorescence intensity, median value in FL1-H = $6 \cdot 10^3$). Subpopulations P_1 and P_2 presented a difference in their specific growth rates in 96 - well plates in double selective medium (*i.e.* gentamicin + kanamycin) with 0.09 ± 0.03 h^{-1} and 0.05 ± 0.01 h^{-1}, respectively (Boy et al., 2020).

Successive batches

First, a batch culture was led at 30°C in order to set the reference condition. This reference condition was characterized by 100 % eGFP - positive cells whose fluorescence intensity distribution was centered on the median of the subpopulation P_2 (= $6 \cdot 10^3$). Then, successive batch cultures were carried out in the same bioreactor at 37°C until the three subpopulations P_0, P_1 and P_2 as defined above appeared. Then, chemostat was started at a dilution rate of 0.05 h^{-1}.

Growth rate during successive batches varied significantly depending on the culture conditions applied (**Table 2**). At 30°C, growth rate was maintained at 0.25 ± 0.01 h^{-1}, which was consistent with optimal culture conditions for this strain. Then, during the first batch at 37°C, the specific growth rate dropped to 0.06 ± 0.01 h^{-1}. This was the lowest specific growth rate observed, since it increased in the next batches from 0.15 ± 0.01 to 0.22 ± 0.01 h^{-1}. So, in the last 37°C - batch, the specific growth rate was only 20 % lower to its value at 30°C.

At the end of the batch at 30°C, the whole cell population remained stable mainly in the subpopulation P_2 gate (**Figures 4a** & **5**), corresponding to the fluorescence intensity distribution under optimal culture conditions. The fluorescence intensity distribution remained symmetric and narrow around the median until the end of the 30°C batch (**Figure 5**).

At the beginning of the first 37°C batch, the median of the fluorescence intensity distribution quickly reached $4 \cdot 10^3$ again in the FL1-H channel. The distribution range was wider than during the 30°C batch. Between 0 and 15 cell generations, the fluorescence intensity distribution remained mostly in the P_2 subpopulation gate (**Figure 5**), but its distribution range increased throughout this time-period (**Figure 4a**). After 15 cell generations, the distribution range increased drastically towards the lower fluorescence intensity, which was confirmed by the increase in the percentage of P_1 fluorescent cells (**Figure 6**). After 30 cell generations, subpopulations P_1 and P_2 were clearly obtained, each one representing approximately 50 % of the eGFP-positive cell population. At that stage, it was decided to switch to chemostat mode.

Plate count was performed at the end of each batch (**Figure7b**). For flow cytometry measurements, only endpoints of each batch were shown (**Figure 7a**). The results for flow cytometry and plate count analysis gave cell concentrations comprised in the same order of magnitude. During successive batches, cell concentration reached around 10^{10} cells·mL^{-1} both by plate count and flow cytometry.

During the successive batches (until 30 generations), the decimal reduction rate (**Figure 7d**) obtained for Gen^RKan^R cells remained close to zero, meaning that all cells present in the bioreactor were bearing the plasmid, even without selection pressure in the bioreactor. Decimal reduction rate for P_2-cells also remained close to zero (**Figure 7c**), but this value started increasing after 15 cell generations up to 0.25. This corresponded to the decrease of the decimal reduction rate for P_1 and P_0 - cells. During the first 15 generations, the decimal reduction rate for P_1 and P_0-cells was higher, around 1.0-1.5 and 1.5-2.2 respectively.

Chemostat at 0.05 h^{-1}

First, a low dilution rate of 0.05 h^{-1} was set, which was close to the lowest specific growth rate obtained during successive batches at 37°C and close to the specific growth rate of P_2-cells (0.07 ± 0.02 h^{-1}) determined on selective medium (gentamicin + kanamycin) in 96 - well plates (Boy et al., 2020). The 0.05 h^{-1} - chemostat was carried out at 37°C for 340 h, corresponding to 27 cell generations. At the macroscopic level, the total biomass concentration expressed as dry cell weight and OD_{600nm} was maintained constant at 5 $g_{CDW} \cdot L^{-1}$ (*i.e.* 2.5 OD_{600nm}). In addition, no significant changes of metabolism were identified based on extracellular metabolites (*i.e.* no metabolites detected by HPLC) and exhausted gas analyses. Based on those macroscopic analyses, the steady state was reached after 35 generations (7.2 generations after the start of 0.05 h^{-1}-chemostat) and still settled after 20 more generations.

Nevertheless, based on single-cell level analysis, it was possible to show an evolution of the distribution of the different subpopulations within the culture stabilized at a stable total biomass concentration.

Two phases could be observed concerning the evolution of fluorescence intensity distribution. First, between 30 and 45 cell generations, fluorescence intensity distribution was maintained at the proportion 20 % P_2, 60 % P_1 and 20 % P_0 (**Figure 6**). At the beginning of the 0.05 h^{-1}-chemostat (*i.e.* between 30 and 33 generations), an increase in the subpopulation P_0 (40 %) was observed to the detriment of the subpopulations P_2 (10 %) and P_1 (50%) (**Figures 5** & **6**), as shown in the boxplots on fluorescence intensity distribution (**Figure 4b**). Over the same time period (*i.e.* 30 to 45 cell generations), P_1–cells decimal reduction rate remained rather low (under 0.20) while it increased transiently for P_2 -cells up to 0.75 (**Figure 7c**). Meanwhile, the decimal reduction rate for kanamycin-resistant cells remained rather low, under 0.20 (**Figure 7d**). Second, between 45 and 55 cell generations, the proportion of the P_2 subpopulation increased from 40 to 60 %, while the proportion of the subpopulations P_0 (5 %) and P_1 (35 %) decreased (**Figure 6**). The fluorescence intensity distribution was centered on the P_2 cell gate with a shoulder in the P_1 cell gate (**Figure 5**; cytogram at 54 generations), and boxplot median ($2 \cdot 10^3$) and mean values ($2.5 \cdot 10^3$) stabilized in FL1-H channel. The overall plasmid-expressing population (eGFP-positive and kanamycin resistant) showed a low decimal reduction rate (**Figures 7 c** & **d**), and the plasmid-based eGFP remained expressed in most cells. This was consistent with the high stable fluorescence intensity distribution in single-cells (**Figure 4b**).

Cell concentration (**Figure 7a**) decreased and stabilized around $7 \cdot 10^8$ cells$\cdot mL^{-1}$ at steady state by flow cytometry. By plate count, cell concentration decreased regularly throughout the cultivation until it reached $1 \cdot 10^9$ cells$\cdot mL^{-1}$ at the end of the first chemostat cultivation.

Therefore, by decreasing the dilution rate to 0.05 h^{-1}, chemostat mode favored the appearance of the subpopulation P_2, which exhibited the highest fluorescence intensity distribution, after 10 numbers of residence time corresponding to 15 generation growing under such condition.

Chemostat at 0.10 h^{-1}

A higher dilution rate of 0.10 h^{-1} was then applied in this experiment. Chemostat was carried out at 37°C and 0.10 h^{-1} for 160 h, corresponding to 23 cell generations (16 hydraulic residence time). As exposed beforehand on macroscopic data, the total biomass concentration was maintained constant at 5 $g_{CDW} \cdot L^{-1}$. Likewise, no significant changes in metabolism were identified based on extracellular metabolites and exhausted gas analyses.

Based on those macroscopic analyses, steady state was reached at 62 generations (7.2 generations after the start of 0.10 h^{-1}-chemostat) and maintained for 23 cell generations.

Between 55 and 62 cell generations (*i.e.* 5 residence times), boxplots showed that the distribution range remained the same width (**Figure 4c**). However, the boxplots themselves were symmetrically transposed by following median / mean increase. This was consistent with the observation, that fluorescence intensity distribution slipped symmetrically through a higher median value in the P_2 cells gate (**Figure 5**) and that the proportion of P_0 and P_1 - cells continued to decline, while the proportion of P_2 cells increased (**Figures 5** & **7a**). Once steady state was reached at 62 generations (*i.e.* 7.2 residence time), boxplots were reproducibly centered on the P_2 - subpopulation (**Figures 4c** & **5**). It was interesting to note that fluorescence intensity distributions median was significantly higher at the end of the 0.10 h^{-1} - chemostat ($1 \cdot 10^4$ in FL1-H) compared to the 0.05 h^{-1} - chemostat ($5 \cdot 10^3$ in FL1-H) (**Figure 4d**) even if they were both mainly included in the P_2 - gate.

On the one hand, the cell concentration measured by flow cytometry increased slightly and stabilized at the steady state at $4 \cdot 10^9$ cells·mL^{-1} (**Figure 7a**). On the other hand, the cell concentration measured by plate count decreased significantly from 1.10^9 to 8.10^7 cells·mL^{-1}. The main reason could lie in the loss of cell cultivability due to the prolonged exposure at 37°C (620 hours from batches to chemostat) and to the higher intracellular eGFP concentration for the P_2 population at 0.10 h^{-1} dilution rate (FL1 median $1 \cdot 10^4$, compared to FL1 median $5 \cdot 10^3$ for P_2 population at 0.05 h^{-1}). Too high, an intracellular concentration of eGFP could indeed be toxic for the cells.

Therefore, increasing the dilution rate from 0.05 to 0.10 h^{-1} favored the maintenance of the P_2 subpopulation compared to P_1 with an increase in the intracellular eGFP concentration for the P_2 population reaching the value of the reference culture at 30°C.

DISCUSSION

Plasmid curing in *Cupriavidus necator* has been used to study the impact of plasmid-encoded mechanisms (*e.g.* hydrogen utilization (Andersen et al., 1981) and toluene metabolism (Hughes et al., 1984)) on both plasmid-bearing and -free cells, by removing the involved plasmid from host cells. Several plasmid curing strategies have been used, presenting with different efficiency levels and ease of use. Here, a plasmid curing method was intended to generate heterogeneity in a cell population in terms of plasmid expression level. Therefore, a mild plasmid curing strategy inducing this heterogeneity was searched without completely inhibiting cell growth.

Temperature increase and rifampicin addition were selected as curing strategies in batch. Despite its lower reported efficiency, rifampicin was chosen as a disruptor of plasmid transcription in bacteria (Buckner et al., 2018) (Wehrli (1983), with the expectation of obtaining an average efficiency on plasmid curing without drastic growth inhibition. Population heterogeneity was studied by flow cytometry based on eGFP-fluorescence and by plate count based on kanamycin resistance.

The heterogeneity was found more pronounced after a temperature increase (30 to 42°C) whereas almost none was observed after rifampicin addition (50 $mg \cdot L^{-1}$). This result confirmed the low efficiency of rifampicin as a curing agent (Buckner et al., 2018).. The plasmid expression level distribution widened after plasmid curing, especially after temperature increase. This expression level heterogeneity at a single-cell level in response to plasmid curing was not observed in previous works, as plasmid stability measurements were mainly based on mean analysis within the overall population (Andersen et al., 1981; Buckner et al., 2018; Hughes et al., 1984; Monchy et al., 2006; Zaman, 2010).

For temperature increase, cell concentrations calculated by plate count were lower than by flow cytometry. For rifampicin addition, there was no difference. Therefore, there was a cultivability loss during plasmid curing by temperature. These observations were supported by propidium iodide staining of cells; after temperature increase, the percentage of permeabilized cells increased up to 15 %, while it remained zero with rifampicin.

Although plate count data presented higher heterogeneity than flow cytometry data (certainly due to cultivability), its level achieved by both counting methods was still quite low. This might be explained by the fact that cell growth drastically slowed down (- 57 %, rifampicin, - 95 %, temperature 42°C) after plasmid curing induction. An insufficient amount of cell generations may have been generated to observe the plasmid curing phenomenon because of the negative impact of both curing agents on cell replication mechanisms.

So, a temperature of 42°C might have been too stringent for cells. Therefore, in the following experiments temperature was set to 37°C instead, allowing inducing heterogeneity and not drastically inhibiting the growth rate.

This was confirmed during successive batches grown at 37°C where a heterogeneity of plasmid expression was still obtained but with a higher growth. The three fluorescent subpopulations P_0 (low / no fluorescence), P_1 (medium fluorescence) and P_2 (high fluorescence), observed in our previous work during successive flasks subcultures (Boy et al., 2020) were observed. Therefore, successive batches at 37°C were proved to be an

effective strategy to obtain a heterogeneous plasmid expression level distribution. The three distinct fluorescent subpopulations P_0, P_1, P_2 were obtained after 30 cell generations. It took way more cell generations to obtain the three distinct subpopulations in successive batches compared to successive flasks subcultures (*i.e.* 19 cell generations (Boy et al. 2020)). This is most probably due to the fact that flask cultures presented more stringent growth conditions that the conditions for bioreactor cultures where the environment was better controlled. (*i.e.* dissolved oxygen concentration and pH).

The continuous cultivation mode is particularly suitable to analyze stress responses of cell subpopulations in a defined physiological state, at a controlled specific growth rate. Here, chemostat was applied to study the impact of the dilution rate on the plasmid expression level by measuring the eGFP fluorescence, under plasmid-curing conditions. This mode of cultivation had already been used in previous works to show that the level of plasmid expression (*i.e.* plasmid replication rate, plasmid copy number) could be regulated by the dilution rate (*i.e.* growth rate) (Dupoet et al., 1987; Klotsky and Schwartz, 1987; Klumpp, 2011; Koizumi et al., 1985; Lin-Chao and Bremer, 1986; Reinikainen and Virkajärvi, 1989; Ryan and Parulekar, 1991). These studies were based on the overall measurement of plasmid DNA content, plasmid copy number, etc. In the literature, different opinions regarding the impact of dilution rate on the level of plasmid expression can be found, as it strongly depends on the "plasmid vector - host cell" association (Chew et al., 1988; D'Angio et al., 1994). For example, different behaviors could be observed depending on the limiting substrate (glucose, ammonium, phosphate or sulphate) or the medium used for the same association (Chew et al., 1988). On the one hand, increased dilution rates led to a decrease in the plasmid copy number. This is the most common trend, as a lower plasmid copy number results in a lower metabolic load and therefore higher growth rate (Patnaik, 2000). This is the case for *Escherichia coli* K12 with plasmid R1 (Light and Molin, 1982), for *E. coli* Br/A with plasmid pBR322 (Lin-Chao and Bremer, 1986) and for *E. coli* JM13 with plasmid pUC8 (Ryan and Parulekar, 1991). On the other hand, plasmids which confer a growth advantage to host cells are less common but might alter the physiological state of cells to favor growth (Patnaik, 2000). It is the case of the association of *E. coli* K12 with the plasmid pBR322 (Klumpp, 2011; Noack et al., 1981; Reinikainen and Virkajärvi, 1989) and also *Bacillus stearothermophilus* CU21 with the plasmid pLP11 (Koizumi et al., 1985), where the plasmid copy number increases with the growth rate. There is not yet a definitive explanation for this phenomenon, but this behavior generally concerns low copy number plasmids and plasmids whose replication is cell-cycle specific (Patnaik, 2000). It has been reported that the plasmid copy number may increase with increasing dilution rates in bacteria, for plasmids with low to medium

copy number. The plasmid used here, pBBR1MCS-2, is known to be a medium copy plasmid at around 30 copies per cell (Buch et al., 2010).

A plasmid curing strategy by raising the temperature was applied in chemostat, hoping to amplify the phenomenon observed in flasks and batch mode, over an increased number of cell generations. The second objective was to analyze the impact of the dilution rate (*i.e.* growth rate). Chemostat was set at 2 dilution rates (0.05 and 0.10 h^{-1}) at 37°C and analyzed in terms of subpopulations. Those dilution rates were chosen because they covered the range of the specific growth rates of the P_1 and P_2 subpopulations previously determined in 96 - well plates in selective medium (Boy et al., 2020). Moreover, 0.05 h^{-1} was close to the lowest specific growth rate observed in the second successive batch at 37°C (where P_2 - cell were still majority). Even when macroscopic steady states were reached after 5 residence times, variations in the fluorescence intensity distribution could be observed. At 0.05 h^{-1}, the steady state favored the settlement of the subpopulation P_1 (80 %) within 10 cell generations, corresponding to 7 residence times. The cell population in the bioreactor was completely renewed and the remaining P_2 - cells from the batches were gradually washed out. However, after 10 new cell generations, a gradual shift was observed towards the increase of the P_2subpopulation. This could be explained by the fact that cells were able to adapt to these conditions of increased temperature for a number of cell generations at this controlled dilution rate. Therefore, at the subpopulation level, the steady state at dilution rate of 0.05 h^{-1} resulted in a 60: 35 % distribution between subpopulations P_2 and P_1, respectively. The fluorescence intensity median reached at the end of the 0.10 h^{-1} - chemostat ($1 \cdot 10^4$ in FL1-H) was significantly higher than that reached at the end of the 0.05 h^{-1} - chemostat ($5 \cdot 10^3$ in FL1-H), even if still was in the P_2 - gate. So, switching the chemostat dilution rate up to 0.10 h^{-1} resulted in the increase of the subpopulation P_2 over the subpopulation P_1. This suggests that the maximal specific growth rates previously estimated for P_1 and P_2 were largely underestimated in 96 - wells plate, otherwise P_2 would have been washed out of the bioreactor. The nearly homogeneous population (90 % P_2) reached at steady state 0.10 h^{-1} could be the result of a growth - rate dependent increase in the plasmid copy number of the P_1 subpopulation to match to the maximal possible number in the strain for this dilution rate (subpopulation P_2). The subpopulation P_2 was maintained and the fluorescence intensity distribution was very stable over time. The cells were able to cope with this higher dilution rate without the need to decrease the protein production performance in supra - optimal temperature conditions, as was also the case under optimal growth conditions.

CONCLUSIONS

Our study showed that well-controlled plasmid curing conditions can be used to generate heterogeneity in plasmid expression in engineered *C. necator* without completely inhibiting cell growth. For this, it was better to use a temperature increase of 30 to 37 °C instead of adding rifampicin. By applying these conditions, to successive batches, we were able to identify three subpopulations with different levels of plasmid-based eGFP expression through the use of our plasmid-encoded eGFP biosensor. The distribution of these three subpopulations could be modulated in chemostat by changing the dilution rate. The further use of the biosensor should make it possible to study the mechanisms underlying the genesis of heterogeneity within the engineered microorganisms cultivated in a bioreactor.

COMPLIANCE WITH ETHICAL STANDARDS

Competing interests

The authors declare that there are no competing interests.

Ethical approval

Not applicable, since the work does not involve any study with human participants or animals

AUTHORS' CONTRIBUTIONS STATEMENT

CB, JL, SA, NG and SG conceived and designed research. CB conducted experiments and analyzed data. CB wrote the manuscript and JL, SA, NG and SG reviewed it. All authors read and approved the manuscript.

DECLARATION

Funding

Funding was obtained from Doctoral Research Assignments from the French Ministry of Research.

Conflicts of interest/Competing interests

The authors declare that there are no competing interests.

Ethics approval

Not applicable, since the work does not involve any study with human participants or animals.

Consent to participate

Not applicable.

Consent for publication

All authors agreed to publish this work.

Availability of data and material

All data generated or analyzed during this study are included in the present work.

Code availability

Not applicable.

REFERENCES

Andersen, K., Tait, R.C., King, W.R., (1981) Plasmids required for utilization of molecular hydrogen by Alcaligenes eutrophus. Archives of Microbiology 129, 384-390. *10.1007/BF00406468*

Aragao, G., (1996) Production de poly-beta-hydroxyalcanoates par Alcaligenes eutrophus: caractérisation cinétique et contribution à l'optimisation de la mise en oeuvre des cultures. Institut National des Sciences Appliquées de Toulouse PHD.

Bazzicalupo, P., Tocchini-Valentini, G.P., (1972) Curing of an Escherichia coli episome by rifampicin (acridine orange-F + -F - -Hfr-lac). Proceedings of the National Academy of Sciences of the United States of America 69, 298-300. *10.1073/pnas.69.2.298*

Binder, D., Drepper, T., Jaeger, K.E., Delvigne, F., Wiechert, W., Kohlheyer, D., Grunberger, A., (2017) Homogenizing bacterial cell factories: Analysis and engineering of phenotypic heterogeneity. Metabolic Engineering 42, 145-156. *10.1016/j.ymben.2017.06.009*

Black, W.B., Zhang, L., Kamoku, C., Liao, J.C., Li, H., (2018) Rearrangement of Coenzyme A-Acylated Carbon Chain Enables Synthesis of Isobutanol via a Novel Pathway in Ralstonia eutropha. ACS Synth Biol 7, 794-800. *10.1021/acssynbio.7b00409*

Boy, C., Lesage, J., Alfenore, S., Gorret, N., Guillouet, S.E., (2020) Plasmid expression level heterogeneity monitoring via heterologous eGFP production at the single-cell level in Cupriavidus necator. Applied Microbiology and Biotechnology. *10.1007/s00253-020-10616-w*

Buch, A.D., Archana, G., Naresh Kumar, G., (2010) Broad-host-range plasmid-mediated metabolic perturbations in Pseudomonas fluorescens 13525. Appl Microbiol Biotechnol 88, 209-218. *10.1007/s00253-010-2717-x*

Buckner, M.M.C., Ciusa, M.L., Piddock, L.J.V., (2018) Strategies to combat antimicrobial resistance: anti-plasmid and plasmid curing. Fems Microbiology Reviews 42, 781-804. *10.1093/femsre/fuy031*

Budde, C.F., Riedel, S.L., Willis, L.B., Rha, C., Sinskey, A.J., (2011) Production of Poly(3-Hydroxybutyrate-co-3-Hydroxyhexanoate) from Plant Oil by Engineered Ralstonia eutropha Strains. Applied and Environmental Microbiology 77, 2847-2854. *10.1128/aem.02429-10*

Carlquist, M., Fernandes, R.L., Helmark, S., Heins, A.L., Lundin, L., Sorensen, S.J., Gernaey, K.V., Lantz, A.E., (2012) Physiological heterogeneities in microbial populations and implications for physical stress tolerance. Microbial Cell Factories 11. *10.1186/1475-2859-11-94*

Chew, L.C.K., Tacon, W.C.A., Cole, J.A., (1988) Effect of growth conditions on the rate of loss of the plasmid pAT153 from continuous cultures of Escherichia coli HB101. Fems Microbiology Letters 56, 101-104. *10.1111/j.1574-6968.1988.tb03157.x*

Crepin, L., Lombard, E., Guillouet, S.E., (2016) Metabolic engineering of Cupriavidus necator for heterotrophic and autotrophic alka(e)ne production. Metabolic Engineering 37, 92-101. *10.1016/j.ymben.2016.05.002*

Cruz, M.V., Gouveia, A.R., Dionísio, M., Freitas, F., Reis, M.A.M., (2019) A Process Engineering Approach to Improve Production of P(3HB) by Cupriavidus necator from Used Cooking Oil. International Journal of Polymer Science 2019, 2191650. *10.1155/2019/2191650*

D'Angio, C., Béal, C., Boquien, C.-Y., Corrieu, G., (1994) Influence of dilution rate and cell immobilization on plasmid stability during continuous cultures of recombinant strains of Lactococcus lactis subsp. lactis. Journal of Biotechnology 34, 87-95. *https://doi.org/10.1016/0168-1656(94)90169-4*

Delvigne, F., Goffin, P., (2014) Microbial heterogeneity affects bioprocess robustness: Dynamic single-cell analysis contributes to understanding of microbial populations. Biotechnology Journal 9, 61-72. *10.1002/biot.201300119*

di Mauro, E., Synder, L., Marino, P., Lamberti, A., Coppo, A., Tocchini-Valentini, G.P., (1969) Rifampicin sensitivity of the components of DNA-dependent RNA polymerase. Nature 222, 533-537. *10.1038/222533a0*

Dupoet, P.D., Arcand, Y., Bernier, R., Barbotin, J.N., Thomas, D., (1987) Plasmid stability in immobilized and free recombinant Escherichia coli JM105(pKK223-200) - Importance of oxygen diffusion, growth rate, and plasmid copy number. Applied and Environmental Microbiology 53, 1548-1555.

Ewering, C., Heuser, F., Benolken, J.K., Bramer, C., Steinbuchel, A., (2006) Metabolic engineering of strains of Ralstonia eutropha and Pseudomonas putida for biotechnological production of 2-methylcitric acid. Metabolic Engineering 8, 587-602. *10.1016/j.ymben.2006.05.007*

Friedrich, C.G., Bowien, B., Friedrich, B., (1979) Formate and oxalate metabolism in Alcaligenes eutrophus. J Gen Microbiol 115, 185-192. *10.1099/00221287-115-1-185*

Fukui, T., Suzuki, M., Tsuge, T., Nakamura, S., (2009) Microbial synthesis of poly((R)-3-hydroxybutyrate-co-3-hydroxypropionate) from unrelated carbon sources by engineered Cupriavidus necator. Biomacromolecules 10, 700-706. *10.1021/bm801391j*

Garrigues, L., Maignien, L., Lombard, E., Singh, J., Guillouet, S.E., (2020) Isopropanol production from carbon dioxide in Cupriavidus necator in a pressurized bioreactor. New Biotechnology 56, 16-20. *https://doi.org/10.1016/j.nbt.2019.11.005*

Gonzalez-Cabaleiro, R., Mitchell, A.M., Smith, W., Wipat, A., Ofiteru, I.D., (2017) Heterogeneity in Pure Microbial Systems: Experimental Measurements and Modeling. Frontiers in Microbiology 8. *10.3389/fmicb.2017.01813*

Grousseau, E., Lu, J.N., Gorret, N., Guillouet, S.E., Sinskey, A.J., (2014) Isopropanol production with engineered Cupriavidus necator as bioproduction platform. Applied Microbiology and Biotechnology 98, 4277-4290. *10.1007/s00253-014-5591-0*

Gruber, S., Hagen, J., Schwab, H., Koefinger, P., (2014) Versatile and stable vectors for efficient gene expression in Ralstonia eutropha H16. Journal of Biotechnology 186, 74-82. *10.1016/j.jbiotec.2014.06.030*

Grunwald, S., Mottet, A., Grousseau, E., Plassmeier, J.K., Popovic, M.K., Uribelarrea, J.L., Gorret, N., Guillouet, S.E., Sinskey, A., (2015) Kinetic and stoichiometric characterization of organoautotrophic growth of Ralstonia eutropha on formic acid in fed-batch and continuous cultures. Microbial Biotechnology 8, 155-163. *10.1111/1751-7915.12149*

Heins, A.L., Weuster-Botz, D., (2018) Population heterogeneity in microbial bioprocesses: origin, analysis, mechanisms, and future perspectives. Bioprocess Biosyst Eng 41, 889-916. *10.1007/s00449-018-1922-3*
Hoefel, T., Wittmann, E., Reinecke, L., Weuster-Botz, D., (2010) Reaction engineering studies for the production of 2-hydroxyisobutyric acid with recombinant Cupriavidus necator H 16. Applied Microbiology and Biotechnology 88, 477-484. *10.1007/s00253-010-2739-4*
Hughes, E.J., Bayly, R.C., Skurray, R.A., (1984) Characterization of a TOL-like plasmid from Alcaligenes eutrophus that controls expression of a chromosomally encoded p-cresol pathway. Journal of bacteriology 158, 73-78.
Johnson, B.F.R.Y.S., (1971) Dissimilation of Aromatic Compounds by Alcaligenes Eutrophus Journal of Bacteriology 107, 468–475.
Klotsky, R.A., Schwartz, I., (1987) Measurement of cat expression from growth-rate-regulated promoters employing beta-lactamase activity as an indicator of plasmid copy number. Gene 55, 141-146. *10.1016/0378-1119(87)90257-5*
Klumpp, S., (2011) Growth-Rate Dependence Reveals Design Principles of Plasmid Copy Number Control. PLOS ONE 6, e20403. *10.1371/journal.pone.0020403*
Koizumi, J., Monden, Y., Aiba, S., (1985) Effects of temperature and dilution rate on the copy number of recombinant plasmid in continuous culture of Bacillus stearothermophilus (pLP11). Biotechnol Bioeng 27, 721-728. *10.1002/bit.260270522*
Koller, M., Atlić, A., Dias, M., Reiterer, A., Braunegg, G., (2010) Microbial PHA Production from Waste Raw Materials. In: Chen, G.G.-Q. (Ed.), Plastics from Bacteria: Natural Functions and Applications. Springer Berlin Heidelberg, Berlin, Heidelberg, pp. 85-119.
Kovach, M.E., Elzer, P.H., Hill, D.S., Robertson, G.T., Farris, M.A., Roop, R.M., Peterson, K.M., (1995) Four new derivatives of the broad-host range cloning vector pBBR1MCS, carrying different antibiotic resistance cassettes. Gene 166, 175-176. *10.1016/0378-1119(95)00584-1*
Krieg, T., Sydow, A., Faust, S., Huth, I., Holtmann, D., (2018) CO(2) to Terpenes: Autotrophic and Electroautotrophic α-Humulene Production with Cupriavidus necator. Angew Chem Int Ed Engl 57, 1879-1882. *10.1002/anie.201711302*
Light, J., Molin, S., (1982) Expression of a copy number control gene (copB) of plasmid R1 is constitutive and growth rate dependent. Journal of Bacteriology 151, 1129-1135.
Lin-Chao, S., Bremer, H., (1986) Effect of the bacterial growth rate on replication control of plasmid pBR322 in Escherichia coli. Molecular and General Genetics MGG 203, 143-149. *10.1007/BF00330395*
Lu, J.N., Brigham, C.J., Rha, C., Sinskey, A.J., (2013) Characterization of an extracellular lipase and its chaperone from Ralstonia eutropha H16. Applied Microbiology and Biotechnology 97, 2443-2454. *10.1007/s00253-012-4115-z*
Marc, J., Grousseau, E., Lombard, E., Sinskey, A.J., Gorret, N., Guillouet, S.E., (2017) Over expression of GroESL in Cupriavidus necator for heterotrophic and autotrophic isopropanol production. Metabolic Engineering 42, 74-84. *10.1016/j.ymben.2017.05.007*
Monchy, S., Benotmane, M.A., Wattiez, R., van Aelst, S., Auquier, V., Borremans, B., Mergeay, M., Taghavi, S., van der Lelie, D., Vallaeys, T., (2006) Transcriptomic and proteomic analyses of the pMOL30-encoded copper resistance in Cupriavidus metallidurans strain CH34. Microbiology-Sgm 152, 1765-1776. *10.1099/mic.0.28593-0*
Muller, J., MacEachran, D., Burd, H., Sathitsuksanoh, N., Bi, C.H., Yeh, Y.C., Lee, T.S., Hillson, N.J., Chhabra, S.R., Singer, S.W., Beller, H.R., (2013) Engineering of Ralstonia eutropha H16 for Autotrophic and Heterotrophic Production of Methyl Ketones. Applied and Environmental Microbiology 79, 4433-4439. *10.1128/aem.00973-13*

Nangle, S.N., Ziesack, M., Buckley, S., Trivedi, D., Loh, D.M., Nocera, D.G., Silver, P.A., (2020) Valorization of CO2; through lithoautotrophic production of sustainable chemicals in Cupriavidus necator. bioRxiv, 2020.2002.2008.940007. *10.1101/2020.02.08.940007*
Noack, D., Roth, M., Geuther, R., Müller, G., Undisz, K., Hoffmeier, C., Gáspár, S., (1981) Maintenance and genetic stability of vector plasmids pBR322 and pBR325 in Escherichia coli K12 strains grown in a chemostat. Molecular and General Genetics MGG 184, 121-124. *10.1007/BF00271207*
Patnaik, P.R., (2000) An evaluation of models for the effect of plasmid copy number on bacterial growth rate. Biotechnology Letters 22, 1719-1725. *10.1023/A:1005696401254*
Pohlmann, A., Fricke, W.F., Reinecke, F., Kusian, B., Liesegang, H., Cramm, R., Eitinger, T., Ewering, C., Potter, M., Schwartz, E., Strittmatter, A., Voss, I., Gottschalk, G., Steinbuchel, A., Friedrich, B., Bowien, B., (2006) Genome sequence of the bioplastic-producing "Knallgas" bacterium Ralstonia eutropha H16. Nature Biotechnology 24, 1257-1262. *10.1038/nbt1244*
Rakotomalala, R., (2011) Tests de normalité - Techniques empiriques et tests statistiques,. Université Lumière Lyon 2 https://docplayer.fr/424798-Tests-de-normalite-techniques-empiriques-et-tests-statistiques.html.
Reinikainen, P., Virkajärvi, I., (1989) Escherichia coli growth and plasmid copy numbers in continuous cultures. Biotechnology Letters 11, 225-230. *10.1007/BF01031568*
Ryan, W., Parulekar, S.J., (1991) Recombinant protein synthesis and plasmid instability in continuous cultures of Escherichia coli JM103 harboring a high copy number plasmid. Biotechnology and Bioengineering 37, 415-429. *10.1002/bit.260370504*
Tang, R., Weng, C., Peng, X., Han, Y., (2020) Metabolic engineering of Cupriavidus necator H16 for improved chemoautotrophic growth and PHB production under oxygen-limiting conditions. Metabolic Engineering 61, 11-23. *https://doi.org/10.1016/j.ymben.2020.04.009*
Trevors, J.T., (1986) Plasmid curing in bacteria. Fems Microbiology Letters 32, 149-157.
Wehrli, W., (1983) Rifampin: Mechanisms of Action and Resistance. Reviews of Infectious Diseases 5, S407-S411. *10.1093/clinids/5.Supplement_3.S407*
Zaman, M.P., MH.; Akhter MZ., (2010) Plasmid Curing of Escherichia coli Cells with Ethidium Bromide, Sodium, Dodecyl Sulfate and Acridine Orange. Bangladesh Journal of Microbiology 27, 28-31.

LEGEND OF THE FIGURES

Figure 1: Box plot representation of fluorescence intensity distribution of eGFP-positive cells in the FL1-A channel throughout fermentation for the strain Re2133/pCB1 under plasmid curing conditions with rifampicin addition (time (a) and generations (b)) and temperature increase (time (c), generations (d) and magnification between 6 and 7.5 generations (e)).

Figure 2: Cell concentration in cells·L^{-1} for the rifampicin experiment, vs cell generations by plate count (◆ Gen^R and ◆ Gen^R+Kan^R) and flow cytometry (● Single cells and ● eGFP-positive cells) (**a**). Cell concentration in cells·L^{-1} for the temperature experiment, vs cell generations by plate count (◆ Gen^R and ◆ Gen^R+Kan^R) and flow cytometry (● Single cells and ● eGFP-positive cells) (**b**). Decimal reduction rate for the rifampicin (**c**) and temperature (**d**) experiments, vs cell generations by plate count (◆) and flow cytometry (●).

Figure 3: Comparison of extracellular fluorescence intensity and the percentage of permeabilized cells throughout fermentation with addition of rifampicin (**a**) and temperature increase at 37°C (**b**). Legend: (●) % PI-positive cells; (▰) extracellular fluorescence intensity.

Figure 4: Plasmid expression levels represented through fluorescence intensity distribution in the FL1-H channel by boxplots during successive batches at 30 and 37°C (**a**), chemostat at 37°C and 0.05 h^{-1} (**b**) and chemostat at 37°C and 0.10 h^{-1} (**c**). Comparison of plasmid expression level distribution on the last point of the 0.05 and 0.1 h^{-1} chemostats, at respectively, 53 and 75 generations (**d**). Delimitation between successive batches were shown by blue and grey vertical lines.

Figure 5: Evolution of fluorescence intensity distribution in the FL1-H channel at different time of culture.

Figure 6: Percentage of P_2-cells (▰) and P_1-cells (▰) and P_0-cells (▰) by flow cytometry through the number of cell generations, and the number of residence time. Red vertical lines represent the delimitation between fermentation conducts (batch, chemostat).

Figure 7: Cell concentrations vs the number of generations for (**a**) fluorescent cells (●) and total cells (✚) determined by flow cytometry as well as (**b**) Gen^R cells (●) and Gen^RKan^R cells (◆). (**c**) Decimal reduction rate vs the number of generations for P_2-cells (■), P_1-cells (▲), P_0-cells (▼) and for (**d**) Gen^RKan^R cells (●).

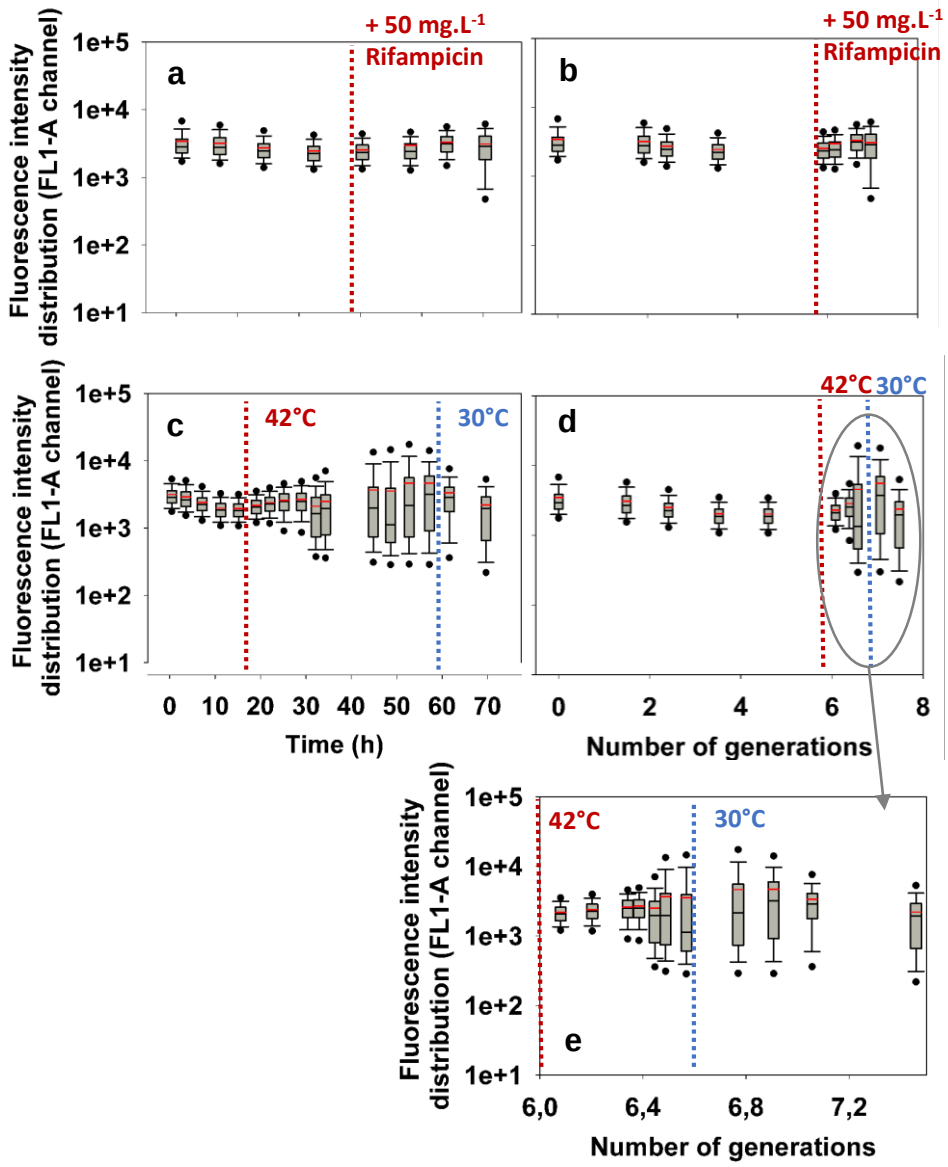
a
+ 50 mg.L-1
Rifampicin
b
+ 50 mg.L-1
Rifampicin
Fluorescence intensity distribution (FL1-A channel)
1e+5
1e+4
1e+3
1e+2
1e+1
c
42°C
30°C
d
42°C
30°C
0 10 20 30 40 50 60 70
Time (h)
0 2 4 6 8
Number of generations
e
42°C
30°C
6,0 6,4 6,8 7,2
Number of generations

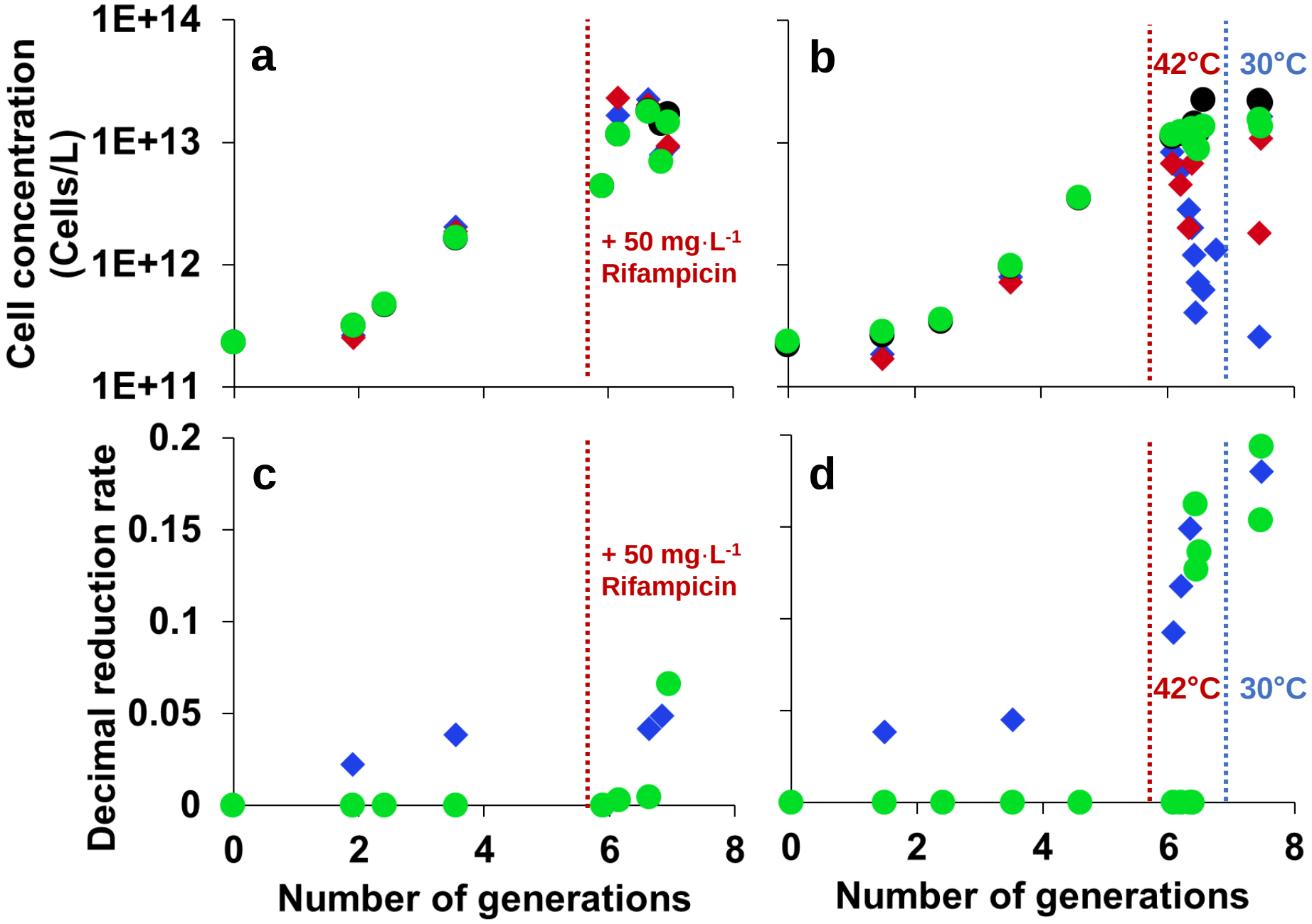
a
b
c
d
Cell concentration (Cells/L)
1E+14
1E+13
1E+12
1E+11
Decimal reduction rate
0.2
0.15
0.1
0.05
0
+ 50 mg·L-1 Rifampicin
42°C
30°C
0
2
4
6
8
Number of generations

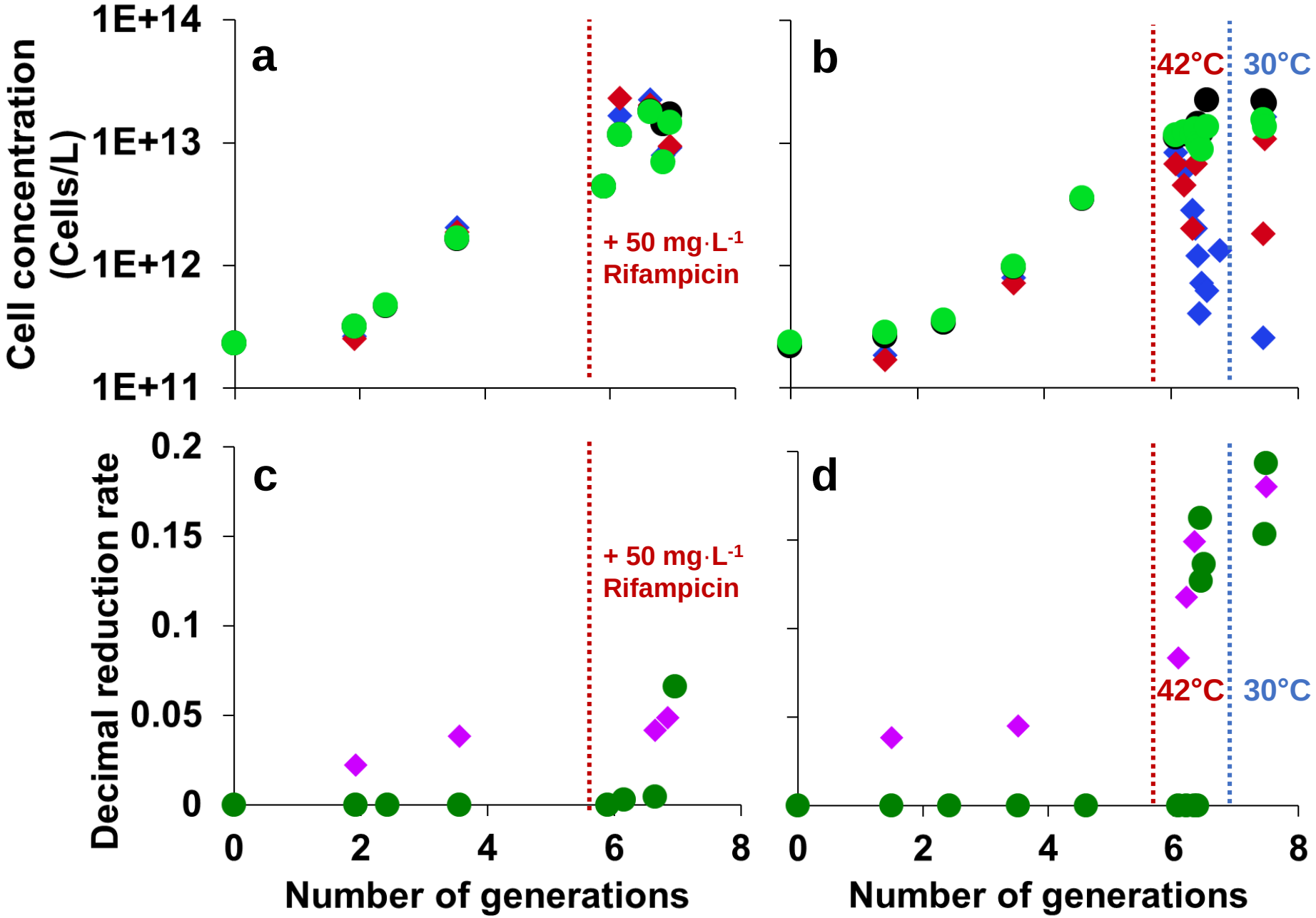
Cell concentration (Cells/L)
1E+14
1E+13
1E+12
1E+11
a
+ 50 mg·L-1 Rifampicin
b
42°C
30°C
Decimal reduction rate
0.2
0.15
0.1
0.05
0
c
+ 50 mg·L-1 Rifampicin
d
42°C
30°C
0
2
4
6
8
Number of generations
Number of generations

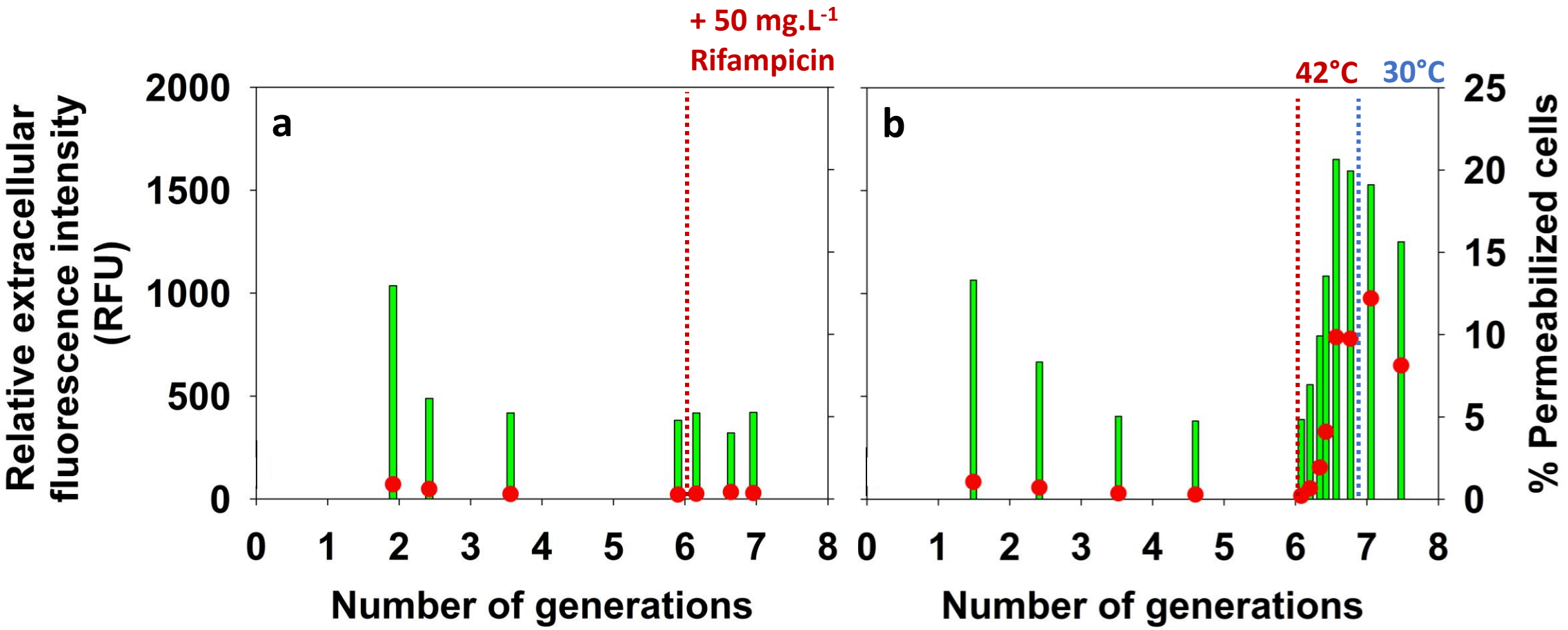
+ 50 mg.L-1
Rifampicin
42°C
30°C
a
b
Relative extracellular fluorescence intensity (RFU)
% Permeabilized cells
2000
1500
1000
500
0
25
20
15
10
5
0
0 1 2 3 4 5 6 7 8
Number of generations
0 1 2 3 4 5 6 7 8
Number of generations

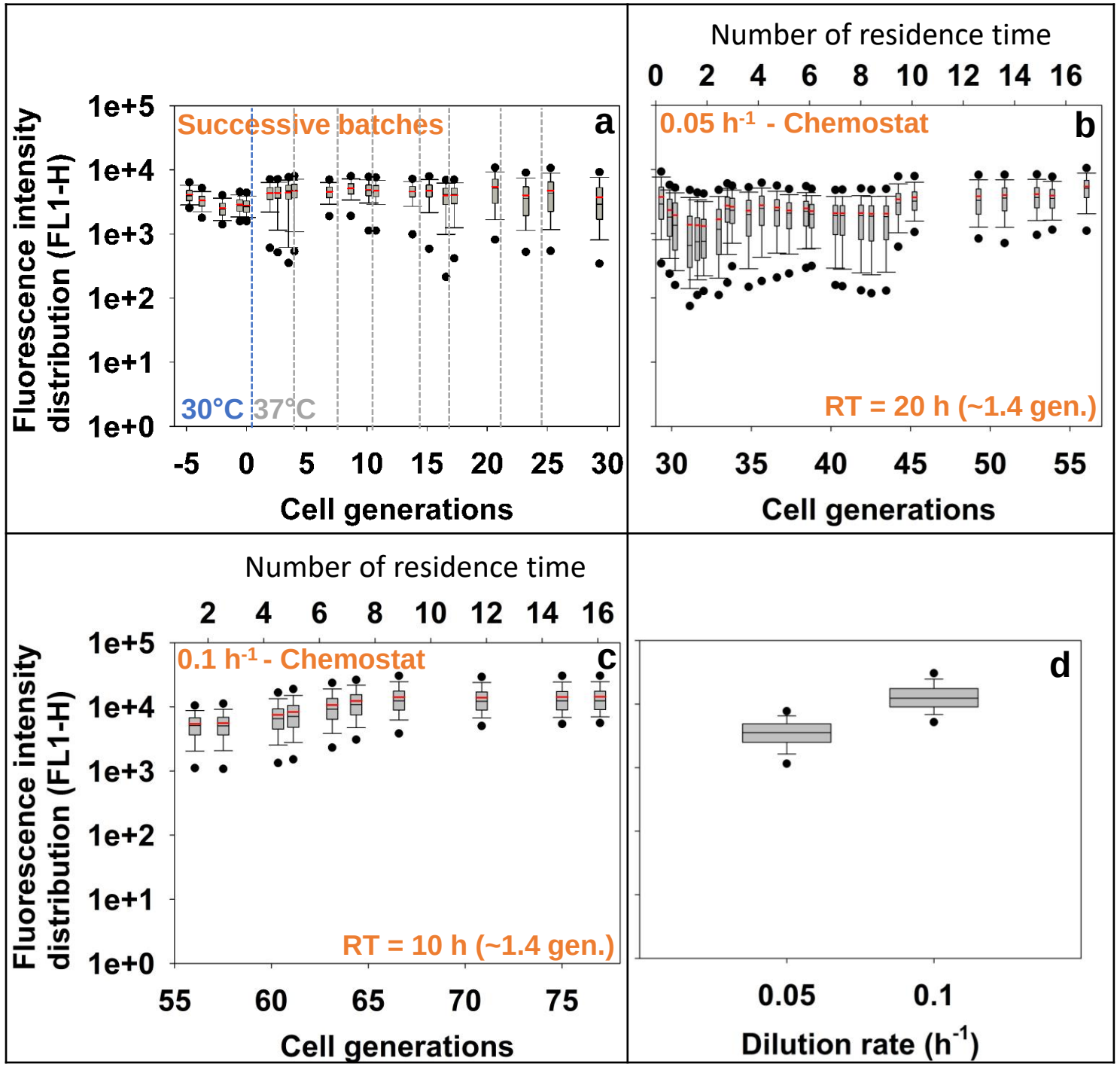
Successive batches
a
30°C
37°C
Fluorescence intensity distribution (FL1-H)
1e+5
1e+4
1e+3
1e+2
1e+1
1e+0
-5 0 5 10 15 20 25 30
Cell generations
Number of residence time
0 2 4 6 8 10 12 14 16
0.05 h-1 - Chemostat
b
RT = 20 h (~1.4 gen.)
30 35 40 45 50 55
Cell generations
Number of residence time
2 4 6 8 10 12 14 16
0.1 h-1 - Chemostat
c
RT = 10 h (~1.4 gen.)
55 60 65 70 75
Cell generations
d
0.05
0.1
Dilution rate (h-1)

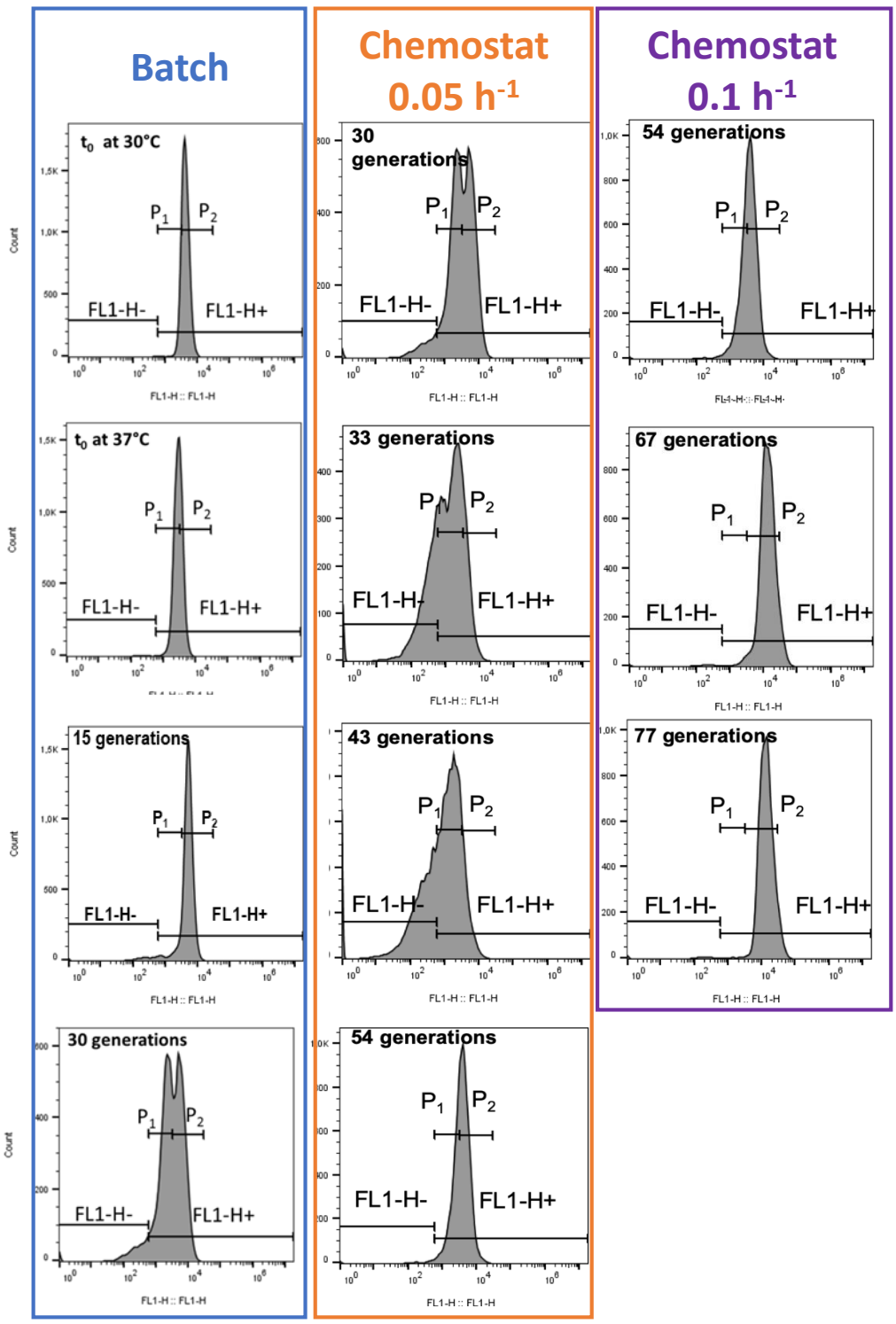
Batch
Chemostat 0.05 h-1
Chemostat 0.1 h-1
t0 at 30°C
30 generations
54 generations
t0 at 37°C
33 generations
67 generations
15 generations
43 generations
77 generations
30 generations
54 generations
P1
P2
FL1-H-
FL1-H+
Count
FL1-H :: FL1-H

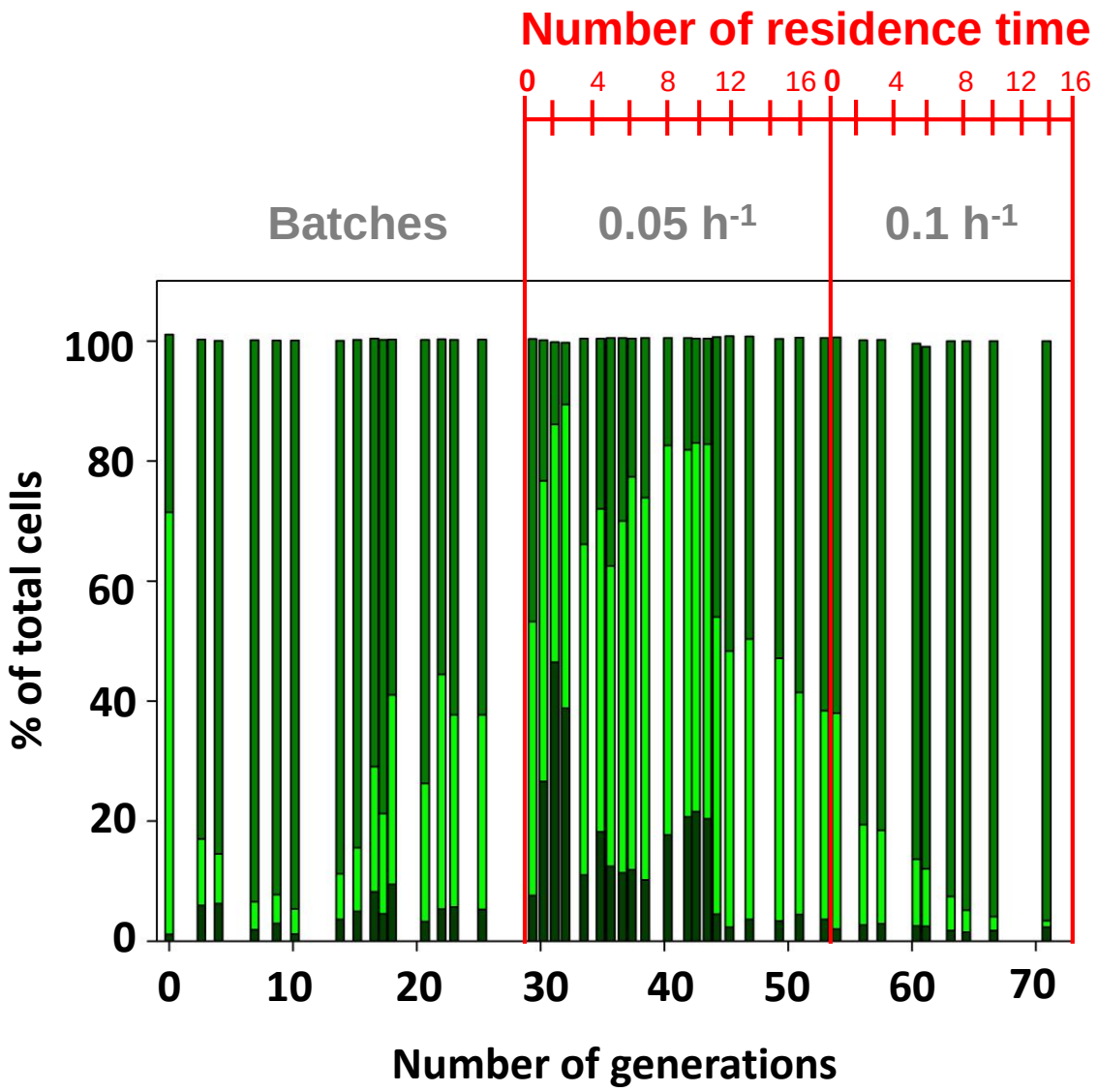
Number of residence time
0
4
8
12
16
0
4
8
12
16
Batches
0.05 h-1
0.1 h-1
100
80
60
40
20
0
% of total cells
0
10
20
30
40
50
60
70
Number of generations

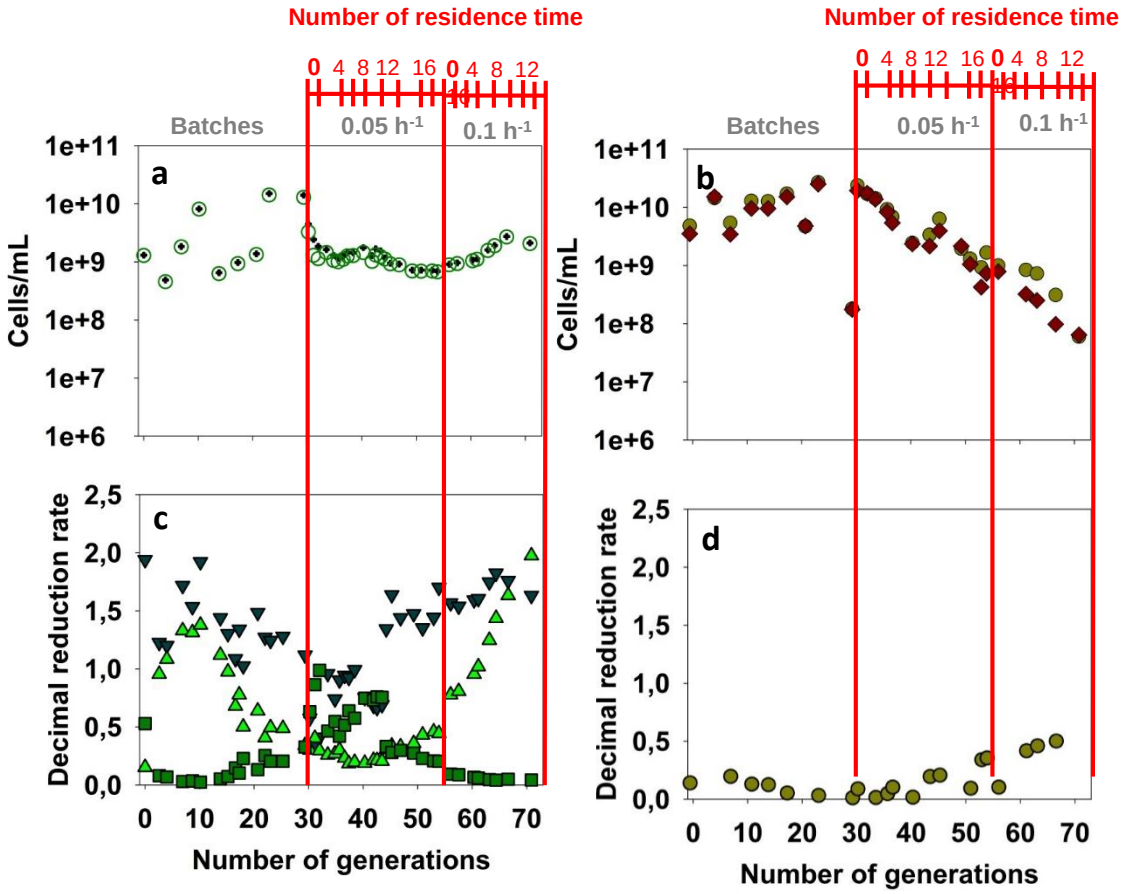
Number of residence time
0 4 8 12 16 0 4 8 12
Batches
0.05 h-1
0.1 h-1
a
b
c
d
Cells/mL
1e+11
1e+10
1e+9
1e+8
1e+7
1e+6
Decimal reduction rate
2,5
2,0
1,5
1,0
0,5
0,0
0 10 20 30 40 50 60 70
Number of generations

TITLE

Study of plasmid-based expression level heterogeneity under plasmid-curing like conditions in *Cupriavidus necator*

AUTHORS

Catherine BOY[1], Julie LESAGE[1], Sandrine ALFENORE[1], Stéphane E. GUILLOUET[1], Nathalie GORRET[1*],

[1] TBI, Université de Toulouse, CNRS, INRA, INSA, Toulouse, France

*CORRESPONDING AUTHOR

Nathalie GORRET

ngorret@insa-toulouse.fr

TBI, Université de Toulouse, CNRS, INRA, INSA, Toulouse, France

135 Avenue de Rangueil – 31077 Toulouse Cedex 04

Table 1

Growth rates and biomass production yields from fructose under plasmid curing conditions in batch cultivations in bioreactors.

	μ (h^{-1})		$Y_{S,X}$ ($g_X \cdot g_S^{-1}$)	
	Optimal growth	**Plasmid curing**	**Optimal growth**	**Plasmid curing**
Rifampicin	0.21 ± 0.04 (0-11h)	0.09 ± 0.01 (19-25h)	0.48 ± 0.01	0.35 ± 0.01
Temperature	0.22 ± 0.02 (0-11h)	*42°C* : 0.009 ± 0.001 (19-45h) *30°C:* 0.04 ± 0.01 (49-62h)	0.47 ± 0.02	0.19 ± 0.02 *(42°C)* 0.45 ± 0.03 *(30°C)*

TITLE

Study of plasmid-based expression level heterogeneity under plasmid-curing like conditions in *Cupriavidus necator*

AUTHORS

Catherine BOY[1], Julie LESAGE[1], Sandrine ALFENORE[1], Stéphane E. GUILLOUET[1], Nathalie GORRET[1*],

[1] TBI, Université de Toulouse, CNRS, INRA, INSA, Toulouse, France

*CORRESPONDING AUTHOR

Nathalie GORRET

ngorret@insa-toulouse.fr

TBI, Université de Toulouse, CNRS, INRA, INSA, Toulouse, France

135 Avenue de Rangueil – 31077 Toulouse Cedex 04

Table 2

Specific growth rates and fluorescence intensity repartition (P0, P1, P2) during successive batches at 30 and 37°C.

Successive batches	μ (h^{-1})	final $\%P_0$	final $\%P_1$	final $\%P_2$
Batch 30°C	0.25 ± 0.01	5	14	81
Batch 37°C: n°1	0.06 ± 0.01	5	14	81
Batch 37°C: n°2	0.18 ± 0.01	2	11	87
Batch 37°C: n°3	0.16 ± 0.01	1	11	88
Batch 37°C: n°4	0.15 ± 0.01	3	10	87
Batch 37°C: n°5	0.17 ± 0.01	5	22	73
Batch 37°C: n°6	0.22 ± 0.01	9	32	59
Batch 37°C: n°7	0.20 ± 0.01	5	32	63
Batch 37°C: n°8	0.20 ± 0.01	7	46	47